IJRAR.ORG E-ISSN: 2348-1269, P-ISSN: 2349-5138

INTERNATIONAL JOURNAL OF RESEARCH AND ANALYTICAL REVIEWS (IJRAR) | IJRAR.ORG

An International Open Access, Peer-reviewed, Refereed Journal

Zinc Ferrite Nanocomposites as Multifunctional Charge-Storage Platforms: Materials Design, Electrochemical Mechanisms and Future Perspectives

Balbhim S. Maharnavar[1], Amol R. Pardeshi[1], Sahadev H. Kangude[1], Vaibhav D. Lohakare[1], Mahesh G. Bagal[2]

[1]Rayat Shikshan Sanstha's, Dada Patil Mahavidyalaya, Karjat, Dist: Ahilyanagar MH, India 414 402.

[2]Rayat Shikshan Sanstha's, S. M. Joshi College, Hadapsar, Pune MH, India 411028.

Abstract:

Zinc ferrite is a promising redox-active transition-metal ferrite for supercapacitor applications, but its practical charge-storage performance is limited by low electrical conductivity, restricted ion transport, and incomplete utilization of electroactive sites. This mini-review summarizes recent advances in $ZnFe_2O_4$-based nanocomposites, focusing on carbonaceous materials, conducting polymers, metal-oxide/ferrite heterostructures, and morphology-controlled architectures. Particular emphasis is placed on the relationships among redox activity, electrical conductivity, electrolyte-ion diffusion, interfacial charge transfer, and structural characteristics. The reported electrochemical performance is discussed in terms of specific capacitance, rate capability, energy and power density, and cycling stability, while distinguishing three-electrode measurements from practical two-electrode devices. Current challenges, including intrinsic conductivity, structural stability, realistic mass loading, scalable synthesis, and mechanistic understanding of charge storage, are also highlighted. Overall, the available evidence indicates that integrating $ZnFe_2O_4$ with conductive phases and ion-accessible architectures can substantially improve charge transport, active-site utilization, and electrochemical durability, making $ZnFe_2O_4$-based nanocomposites promising candidates for advanced supercapacitor electrodes.

Keywords: $ZnFe_2O_4$, Nanocomposites, Supercapacitors, Polymers.

1. Introduction

The increasing demand of renewable energy systems, portable and wearable electronics, electric transportation, and autonomous devices has generated a continuing requirement for electrochemical energy-storage devices which capable of delivering high power, rapid charge-discharge kinetics, and long-term operational stability. Supercapacitors have consequently attracted due to charge-storage characteristics which occupy an intermediate regime between conventional dielectric capacitors and rechargeable batteries. The electrochemical behaviour of a supercapacitor electrode depends on intrinsic redox chemistry, electronic conductivity, accessible surface area, electrolyte penetration, ion-diffusion pathways, and structural stability. The investigate the ferrite-based electrodes has emerged within this broader effort to develop redox-active, compositionally tunable, and potentially low-cost electrode materials [1].

Spinel ferrites, generally represented by MFe_2O_4, constitute an important family of mixed-metal oxides in which the physicochemical properties can be modified through the identity of the divalent cation, cation distribution, crystallite dimensions, morphology, and synthesis conditions. Comparative study of ferrite compositions has reveals that changing the M-site cation can substantially influence structural, magnetic,

electronic, and electrochemical characteristics [2]. The structural flexibility of spinel ferrites enables their integration into different nanoscale architectures, while the presence of transition-metal cations provides opportunities for reversible redox processes. In addition to electrochemical energy storage, $ZnFe_2O_4$-containing materials have been investigated in lithium-ion battery systems, demonstrating the broader relevance of this ferrite to electrochemical energy technologies and highlighting the importance of nanoscale structural control for improving charge-transport properties [3]. Electrophoretically deposited $ZnFe_2O_4$ coatings have also shown that electrode architecture can significantly affect the ferrite phase's electrochemical response, offering an early warning of the significance of regulating active-material distribution and electrode/electrolyte contact [4].

Research in photoelectrochemical and catalytic systems, where control over crystallinity, composition, surface chemistry, and charge-transfer interfaces is necessary to achieve effective electrochemical processes, further demonstrates $ZnFe_2O_4$ versatility [5]. The charge-storage properties of spinel ferrites cannot be regarded independently of their chemical identity and structural characteristics, as comparative studies of various solvothermally prepared metal ferrites have shown that ferrite composition and nanoscale morphology can produce significant differences in electrochemical behaviour [6]. Similar to this, graphene-supported spinel ferrite systems have shown that ferrite redox activity may be combined with a highly conductive carbonaceous phase, this strategy later became crucial for the development of high-performance ferrite-based electrochemical electrodes [7]. Further evidence of carbon-supported ferrites' capacity to produce linked interfacial structures with enhanced electrochemical accessibility has come from studies of manganese- and zinc-ferrite/graphene architectures [8].

Zinc ferrite ($ZnFe_2O_4$) is one of the most appealing spinel ferrites for electrochemical energy-storage applications due to its chemically resistant spinel structure and the relative abundance of Zn and Fe. Although $ZnFe_2O_4$ is commonly characterized as a normal-spinel compound, its physicochemical behaviour can be affected by defects, replacement, heat treatment, and nanoscale processing that alters the cation distribution. Through surface alteration and morphological engineering, its qualities can be further altered. Research on $ZnFe_2O_4$ nanostructures has shown that surface features, defect structure, crystallite size, and particle shape are all highly dependent on synthesis conditions and can significantly affect the material's functional capabilities [9]. Similar evidence of the significance of surface modification and interfacial passivation in regulating charge-transfer processes has been provided by the creation of $ZnFeO_4$ nanorods and related nanostructured photoelectrodes [10].

When used as an electrochemical charge-storage material, pure $ZnFe_2O_4$ has a number of drawbacks despite these advantageous properties. It's very low electrical conductivity, which can raise internal resistance and hinder electron transit across the active-material network, is one of the main problems. At high current densities or scan speeds, when quick electronic and ionic transport is necessary to effectively use the available redox-active sites, this restriction becomes very significant. One of the main reasons for linking the ferrite with electrically conductive materials is the precise identification of $ZnFe_2O_4$'s poor conductivity as a factor limiting its rate capacity [11]. Further evidence that charge-transfer kinetics and electrochemical accessibility may be controlled by altering composition and interfacial chemistry comes from related Zn-containing ferrite systems and mixed-metal multilayer structures [12]. Specifically, $ZnFe_2O_4/graphene-nanoplatelet$ nanocomposites show how adding a conductive carbon phase can enhance the ferrite's electrochemical reactivity by creating more advantageous electronic routes and making active areas more accessible [13].

The propensity of nanoscale $ZnFeO_4$ particles to agglomerate, which might lower the effective electrochemically accessible surface area and obstruct electrolyte penetration, is another significant constraint. Because it reduces typical diffusion distances and raises the surface-to-volume ratio, nano structuring is beneficial, nevertheless, these advantages may be partially offset by unchecked particle development or aggregation. One method for altering ferrite structure and physicochemical qualities while perhaps regulating active-site properties is cation substitution [14]. Similar to this, $ZnFe_2O_4$ nanostructures made by various synthetic methods show that their functional behavior is strongly correlated with their shape, crystallinity, and surface architecture [15]. Sol-gel derived zinc ferrite material synthesis methodology can influence crystallographic characteristics and electrochemical properties [16]. Electrodeposition provides another route for controlling $ZnFe_2O_4$ film morphology and interfacial contact with the underlying electrode, thereby offering opportunities for reducing transport limitations associated with conventional particulate electrodes [17].

The importance of composition, morphology, and heterointerface become more apparent when $ZnFe_2O_4$ is combined with other metal oxides or electrochemically active phases. $ZnFe_2O_4/TiO_2$ architectures, for example, demonstrate how coupling two oxide phases can generate interfacial structures with modified charge-transfer characteristics [18]. In supercapacitor-oriented systems, ternary architectures containing Ni-Zn ferrite, reduced graphene oxide, and conducting polymer components provide a particularly relevant multiple functional phases can be integrated to simultaneously address conductivity, surface accessibility, and electrochemical activity [19]. Electrochemically $zinc-iron\ oxyhydroxide/ZnFe_2O_4$ heterostructures further demonstrate that deliberately designed interfaces which modify the electrochemical environment and improve the accessibility of redox-active regions [20]. These studies indicate that the performance of $ZnFe_2O_4$-containing electrodes is governed by the intrinsic properties of the ferrite phase rather, it emerges from the coupled effects of composition, morphology, interfacial chemistry, conductivity, and electrolyte accessibility.

The ferrite literature provides useful evidence for understanding these structure-property relationships. $ZnFe_2O_4$-based materials have been investigated in photocatalytic systems, where surface area, defect chemistry, phase composition, and interfacial charge transfer play important roles [21]. Mixed $Mn-Zn$ ferrites embedded in silica demonstrate how incorporation of ferrite nanoparticles into a matrix can influence particle growth, dispersion, and surface properties [22]. Related $Zn-Co$ ferrite systems further show that manipulating the distribution and oxidation-state environment of transition-metal cations can alter functional properties and electrochemical behaviour [23]. $Cobalt-doped\ ZnFe_2O_4$ thin films provide the evidence that substitution at the cationic sites can modify the electronic properties of the ferrite framework [24]. These observations reveal to supercapacitor design because electronic structure and redox accessibility directly influence the kinetics of Faradaic charge storage.

The development of $ZnFe_2O_4$-based nanocomposites therefore provides a rational strategy for overcoming the limitations of the pristine material. Carbonaceous components can establish continuous electron-conduction networks, suppress ferrite aggregation, increase electrolyte-accessible surface area, and improve structural integrity. Carbon quantum dot/ferrite systems further demonstrate how nanoscale carbon-ferrite interactions can modify interfacial electrochemical properties [25]. Although analogous studies on other ferrites, such as $NiFe_2O_4$, demonstrate the effects of catisson substitution and structural modification, they also provide useful principles for understanding how chemical substitution can alter spinel electronic and structural characteristics [26]. Substitution-induced modification of ferrite materials has similarly been investigated in other electrochemical systems, emphasizing the general importance of controlling cation chemistry rather than treating the spinel lattice as chemically invariant [27].

At the device level, the development of supercapacitors increasingly involves rational integration of active materials with conductive scaffolds and complementary charge-storage components. Contemporary studies of electrochemical energy-storage devices emphasize the importance of matching electrode chemistry with the appropriate charge-storage mechanism and device architecture [28]. Two-dimensional materials have also emerged as important components of advanced supercapacitor electrodes because of their high surface accessibility and electronic properties, providing a conceptual basis for integrating low-dimensional conductive phases with ferrite nanoparticles [29]. The successful integration of ferrite nanoparticles with hollow or porous carbon-based architectures further demonstrates that hierarchical structural design can simultaneously improve electrolyte accessibility, active-site utilization, and mechanical stability [30].

The importance of rational interface and architecture design extends beyond conventional aqueous supercapacitor electrodes. Complex oxide architectures used in electrochemical energy technologies demonstrate that controlling nanoscale interfaces and phase connectivity can strongly influence transport properties [31]. Spinel ferrite systems exhibiting intrinsic pseudocapacitive characteristics provide additional evidence that the electrochemical response of ferrites is closely related to their composition, electronic structure, and accessible redox states [32]. High-entropy spinel oxides further demonstrate the possibility of using multination compositional complexity to manipulate the electronic and catalytic properties of spinel frameworks [33]. Likewise, graphene-based nanocomposite aerogels and other three-dimensional conductive architectures demonstrate the potential of hierarchical carbon networks for improving electron transport and electrolyte accessibility in oxide-based electrodes [34].

The relationship between composition, defect chemistry, interfaces, and electrochemical kinetics is therefore central to the rational development of ferrite electrodes. Studies involving substituted mixed oxides demonstrate that changes in cation occupancy and local coordination can influence electronic transport and

electrochemical activity [35]. High-entropy and multicomponent spinel systems provide additional evidence that compositional complexity can be deliberately exploited to tune the functional properties of oxide frameworks [36]. Three-dimensional graphene/metal-oxide architectures further emphasize the importance of conductive percolation networks and hierarchical porosity in achieving efficient utilization of redox-active oxide nanoparticles [37]. These concepts are particularly relevant to $ZnFe_2O_4$ because its electrochemical performance can be improved when the ferrite phase is appropriately dispersed and electronically coupled to a conductive framework rather than simply increasing the quantity of ferrite.

The electrochemical behaviours of spinel ferrites are strongly influenced by cation valence and crystallographic site occupancy. Systematic studies of XFe_2O_4 ferrites have demonstrated that the valence-change capability and geometrical occupation of substitutional cations can determine the extent and nature of pseudocapacitive charge storage [38]. This finding provides an important mechanistic foundation for interpreting the electrochemical response of $ZnFe_2O_4$-based materials and for distinguishing genuine Faradaic contributions from purely double-layer processes. The synthesis and nanostructuring of spinel ferrites are also strongly dependent on wet-chemical processing conditions, precursor chemistry, nucleation, crystal growth, and thermal treatment, all of which ultimately influence particle size, phase purity, defects, and surface characteristics [38]. Consequently, controlling synthesis parameters is not merely a means of obtaining a desired morphology, it represents a fundamental route for controlling the electrochemically active structure.

Sustainability and practical electrode provide additional dimensions to the development of $ZnFe_2O_4$-based supercapacitors. The conversion of zinc-carbon battery waste into carbonaceous electrode components demonstrates the possibility of integrating waste-derived materials into electrochemical energy-storage device [39]. Related investigations of manganese ferrites containing transition-metal substitutions illustrate how deliberate modification of ferrite composition can influence electrode behaviour in redox-active electrolytes [40]. Particularly relevant to the present review, $ZnFe_2O_4@carbon$ core-shell structures integrated with reduced graphene oxide demonstrate the effectiveness of combining nanoscale $ZnFe_2O_4$, protective/conductive carbon, and a two-dimensional conductive network within a single hierarchical architecture [41]. Such architectures directly address several limitations of pristine $ZnFe_2O_4$ by improving electronic connectivity, limiting particle aggregation, and increasing the accessibility of electrochemically active interfaces.

$ZnFe_2O_4$ should not be considered simply as an isolated redox-active oxide, but rather as a tenable functional component whose electrochemical performance depends on the coordinated design of composition, crystallographic structure, particle morphology, porosity, conductivity, interface chemistry, and electrolyte accessibility. The principal challenge is therefore to construct nanocomposite architectures in which $ZnFe_2O_4$ provides accessible Faradaic activity while the accompanying conductive or structurally functional phase facilitates rapid electron transport, efficient ion diffusion, and long-term structural retention. This design philosophy is consistent with the broader understanding that ferrite electrochemistry can vary substantially with composition and electrolyte, and that reported capacitance values must therefore be interpreted together with measurement configuration and charge-storage mechanism.

This mini-review, $ZnFe_2O_4$-based nanocomposite electrodes for supercapacitor applications shows the strategies for morphology and composition control, incorporation of conductive carbonaceous and polymeric phases, heterointerface engineering, charge-storage mechanisms, and the resulting structure, electrochemical property relationships.

2. Zinc Ferrite: Fundamental Features and Charge-Storage Chemistry

2.1 Crystal Structure and Physicochemical Characteristics of $ZnFe_2O_4$

Zinc ferrite ($ZnFe_2O_4$) is a ternary transition-metal oxide belonging to the spinel ferrite family, generally represented by the structural formula AB_2O_4. The $ZnFe_2O_4$ lattice adopts a cubic spinel framework in which O^{2-} anions form a closely packed face-cantered arrangement, while the cations occupy a fraction of the available tetrahedral (A) and octahedral [B] interstitial sites. Experimentally, $ZnFe_2O_4$ is commonly described as a predominantly normal spinel, with Zn^{2+} preferentially occupying tetrahedral A sites and Fe^{3+} predominantly occupying octahedral B sites. This structural assignment is consistent with the XRD and spectroscopic observations reported for $ZnFe_2O_4$-based materials in this literature [2,4,16,41]. In the electrophoretically deposited $ZnFe_2O_4$ nanoparticles, the characteristic reflections at approximately $29.9°, 35.3°, 42.9°, 53.2°, 56.7°, and\ 62.2°$ were indexed to the

$(220), (311), (400), (422), (511), and\ (440)$ planes of the cubic spinel phase, respectively, confirming the formation of crystalline $ZnFe_2O_4$ [4].

The nominal cation arrangement can therefore be represented as $(Zn^{2+})A[Fe^{3+}{}_2]BO_4$. However, the term "normal spinel" should not be interpreted as an absolutely fixed cation configuration. Cation redistribution between tetrahedral and octahedral sublattices can occur depending on synthesis temperature, precursor chemistry, particle size, thermal history, and nanoscale surface effects. The cobalt-substituted $ZnFe_2O_4$ study, explicitly reports that substitution can modify the distribution of cations between tetrahedral and octahedral sites and can simultaneously alter lattice parameters and crystallite dimensions [2]. This is particularly important for nanoscale $ZnFe_2O_4$ because the large surface-to-volume ratio provides a greater fraction of under-coordinated surface sites and can facilitate deviations from the bulk-equilibrium cation distribution. The crystallographic characteristics are closely connected with the nanoscale physicochemical properties of $ZnFe_2O_4$. $zinc\ ferrite$ crystallite sizes vary substantially depending on the synthesis route. $ZnFe_2O_4$ prepared through the solvothermal route exhibited a crystallite size of approximately 34.4 nm, whereas another $ZnFe_2O_4$ preparation yielded approximately 25 nm crystallites [6,16]. More importantly for electrochemical applications, the electrophoretically deposited $ZnFe_2O_4$ consisted of relatively uniform spherical nanoparticles with an average size of $6.8 \pm 1.2\ nm$ [4]. Such differences in crystallite and particle dimensions are significant because they modify the ratio of surface to bulk atoms, accessible active sites, defect concentration, electrolyte penetration, and characteristic electron/ion transport distances.

The surface chemistry of $ZnFe_2O_4$ is associated with its metal-oxygen framework. FTIR analysis of the ferrites examined which revealed metal-oxygen vibrations associated with tetrahedral and octahedral coordination environments, supporting the formation of the spinel ferrite framework [6]. Therefore, the electrochemical behaviour of $ZnFe_2O_4$ should be understood as a consequence of the coupled effects of its spinel lattice, cation distribution, metal-oxygen bonding, crystallite size, surface structure, and porosity, rather than being attributed to a single redox centre.

2.2 Role of $Zn^{2+}/Fe^{2+}/Fe^{3+}$ redox chemistry

The charge-storage chemistry of $ZnFe_2O_4$ is more appropriately described as a mixed surface/interfacial Faradaic process involving the metal-oxygen framework, rather than as a simple Zn^{2+}/Zn^{3+} redox couple. In this supercapacitor study of $ZnFe_2O_4$ coatings, distinct anodic and cathodic features were observed in the cyclic-voltammetry. The attributed these features to Faradaic reactions associated with $M-O/M-O-OH$ $(M = Zn\ or\ Fe)$ surface species and interpreted the resulting response as pseudocapacitive [4].

The study associated the pseudocapacitive response with reversible interaction between Fe^{3+} −containing surface sites and electrolyte K^+ ions, together with intercalation/deintercalation processes occurring at the porous electrode/electrolyte interface [4]. This observation indicates that the electrochemical response is strongly dependent on surface-accessible metal-oxygen sites and electrolyte-ion transport, rather than being controlled exclusively by bulk $ZnFe_2O_4$. A scientifically important distinction should be made concerning Fe^{2+}/Fe^{3+} chemistry. The nominal stoichiometric normal-spinel structure of $ZnFe_2O_4$ is conventionally described using $Zn^{2+}\ and\ Fe^{3+}$, i.e., $Zn^{2+}Fe^{3+}{}_2O_4$. Therefore, it would be inaccurate to state that pristine, stoichiometric $ZnFe_2O_4$ inherently contains a large population of Fe^{2+} ions. Fe^{2+} can arise under particular synthesis, defect, reduction, nanoscale, or electrochemical conditions, and mixed Fe^{2+}/Fe^{3+} states may consequently contribute to charge transport in appropriately modified $ZnFe_2O_4$. However, this review predominantly identifies Fe^{3+} rather than directly demonstrating Fe^{2+} in pristine $ZnFe_2O_4$. XPS analysis of the $ZnFe_2O_4@C/RGO$ material identified $Fe^{3+}\ and\ Zn^{2+}$, with the $Fe\ 2p$ features associated with Fe^{3+} in the $ZnFe_2O_4$ structure [41]. the role of Fe^{2+} should be presented as a possible mixed-valence contribution under non-ideal or modified conditions, rather than as the defining redox state of pristine $ZnFe_2O_4$. This distinction becomes particularly important when interpreting electrochemical mechanisms because an observed redox peak does not by itself establish a specific Fe^{3+}/Fe^{2+} conversion unless supported by appropriate spectroscopic or structural evidence.

In addition, the electrochemical response can involve hydroxylated surface species. The observation of $M-O/M-O-OH$ related Faradaic features in $ZnFe_2O_4$ electrodes which indicates that electrolyte-derived hydroxyl species can participate in surface redox chemistry [4]. The $ZnFe_2O_4/g-C_3N_4$ study provides complementary evidence: oxidation and reduction peaks were attributed to reactions involving

Zn/Fe centers and OH^- species, while the composite exhibited stronger electrochemical response than pristine $ZnFe_2O_4$ [9].

2.3 Contribution of Surface and Faradaic Reactions to Pseudocapacitance

The electrochemical response of $ZnFe_2O_4$ differs fundamentally from that of a purely EDLC carbon electrode because the ferrite can undergo reversible Faradaic reactions at electrochemically accessible sites. In EDLCs, charge accumulation is predominantly electrostatic and occurs through ion adsorption at the electrode/electrolyte interface. In contrast, the $ZnFe_2O_4$ electrodes investigated which exhibit redox features in their cyclic-voltammetry curves, demonstrating a substantial Faradaic component [4,9,13]. The $ZnFe_2O_4/graphene$-nanoplatelet study explicitly distinguishes EDLC-type charge accumulation from pseudocapacitive storage arising from reversible Faradaic reactions and attributes the enhanced electrochemical behaviour of the composite to improved electrode/electrolyte charge-transfer characteristics and graphene conductivity [13].

$ZnFe_2O_4$, the surface region is particularly important because electrolyte ions must reach electrochemically active metal-oxygen sites before Faradaic charge transfer can occur. The $ZnFe_2O_4$ coating study provides direct evidence of this transport dependence: at low scan rate, both the outer and inner regions of the porous electrode were accessible to electrolyte ions, whereas at higher scan rates, ion access became increasingly restricted to the outer regions [4]. Consequently, the measured capacitance decreased with increasing scan rate. this behaviour highlights an important distinction between intrinsic redox activity and experimentally accessible capacitance. A material may contain a large theoretical number of redox-active sites, but only a fraction can contribute to the measured capacitance if electronic conduction or ionic diffusion is kinetically limited. In the $ZnFe_2O_4$ coating study, the relatively low specific capacitance was associated partly with the poor electrical conductivity of $ZnFe_2O_4$, while the scan-rate dependence was linked to progressively incomplete utilization of the internal electrode regions [4].

The importance of surface morphology from $ZnFe_2O_4 - based$ composites. In the $ZnFe_2O_4/g - C_3N_4$ system, incorporation of $g - C_3N_4$ increased the electrochemically active redox contribution and facilitated charge-carrier pathways. The composite exhibited a higher specific capacitance than pristine $ZnFe_2O_4$, with the researchers associating this enhancement with improved OH^- diffusion and a more favorable $ZnFe_2O_4/g - C_3N_4$ interface [9]. $ZnFe_2O_4/graphene$ nanoplatelet nanocomposites exhibited markedly improved electrochemical capacitance compared with the ferrite alone. The enhancement was attributed to the conductive nature of graphene nanoplatelets and the improved electrode/electrolyte charge-transfer interface [13]. Thus, the measured capacitance of $ZnFe_2O_4$ nanocomposites should be viewed as the combined outcome of

1. Faradaic redox reactions at $Zn/Fe - O$ surface sites
2. electrolyte-ion adsorption and interfacial charge accumulation
3. ion insertion/deinsertion into accessible near-surface regions
4. electronic transport through the $ZnFe_2O_4$ network
5. ionic transport through pores and electrolyte-accessible interfaces.

This coupled mechanism explains why the electrochemical performance cannot be predicted solely from the $ZnFe_2O_4$ crystal structure.

2.4 Relationship Between Particle Size, Morphology, and Electrochemical Activity

Particle size and morphology exert a decisive influence on $ZnFe_2O_4$ electrochemical behaviour because they control the electrochemically accessible surface area, diffusion length, porosity, particle connectivity, and density of exposed active sites. Reduction of particle size generally increases the surface to volume ratio and decreases the characteristic distance over which electrolyte ions and electrons must travel. $ZnFe_2O_4$ studies provide direct experimental evidence for this structural dependence. synthesized relatively uniform $ZnFe_2O_4$ nanoparticles with an average diameter of $6.8 \pm 1.2\ nm$ [4]. Such nanoscale dimensions are advantageous because a greater proportion of the material can be exposed to the electrolyte. However, nanosizing alone does not guarantee high capacitance because nanoparticle aggregation, poor electronic connectivity, and excessive electrode thickness can still limit active-site utilization.

The morphology performance relationship is also apparent from the comparative ferrite study of $ZnFe_2O_4$ formed nearly spherical nanoassemblies and exhibited a particle size of approximately 81 nm, while the crystallite dimension was smaller. The researchers observed cluster formation arising from the assembly of smaller particles and demonstrated that ferrite morphology and porosity were strongly dependent on the synthesis conditions [6]. This distinction between crystallite size and secondary particle size is important, electrochemical transport is governed not only by the dimensions of individual crystalline domains but domains assemble into larger aggregates and porous networks. A particularly important consequence of morphology is the balance between surface area and structural connectivity. Highly aggregated nanoparticles can possess a nominally high surface area while simultaneously creating tortuous pathways for electrolyte transport and increasing interparticle electrical resistance. Conversely, a well-connected porous architecture can expose internal surfaces while providing shorter pathways for ion migration. The $ZnFe_2O_4$ coating study demonstrated this principle directly, although the nanoparticles remained nanoscale and were relatively uniformly distributed without obvious agglomeration, the relatively thick electrode still showed strong scan-rate dependence because the inner electrode regions became progressively inaccessible at higher rates [4].

Nanocomposite formation can therefore provide a more effective solution than particle-size reduction alone. In the $ZnFe_2O_4/g-C_3N_4$ system, the $ZnFe_2O_4$ crystallite size decreased from approximately 30 nm for pristine $ZnFe_2O_4$ to 21 nm in the composite, while the researchers associated the structural modification with strong interaction between $ZnFe_2O_4$ and $g-C_3N_4$ [9]. The resulting heterointerface improved electrochemical response by providing more favorable charge-transport and ion-diffusion pathways [9]. An even more sophisticated morphology is obtained by integrating $ZnFe_2O_4$ nanoparticles into core-shell and graphene-based hierarchical architectures. In the $ZnFe_2O_4@C/rGO$ system, $ZnFe_2O_4$ nanoparticles of approximately 15-20 nm were enclosed within a carbon shell and further integrated with reduced graphene oxide. The carbon shell and rGO formed a buffering and conductive network around the ferrite particles, while the $ZnFe_2O_4$ crystalline domains remained approximately 16 nm in the composite [41]. Such an architecture illustrates a central principle for $ZnFe_2O_4$ electrode design, the objective is not simply to minimize particle size, but to maximize the fraction of redox-active material that is simultaneously accessible to electrolyte ions and electronically connected to the current collector.

3. Design Strategies for $ZnFe_2O_4$ −Based Nanocomposites

3.1 $ZnFe_2O_4/Carbon\ Nanocomposites$

The incorporation of carbonaceous materials into $ZnFe_2O_4$ is an effective strategy for modifying the electrochemical behaviour of the ferrite by improving electronic connectivity and creating more favourable electrode/electrolyte interfaces. Fig. 1. Show the $ZnFe_2O_4/Graphene$ morphology with interface [13].

Graphene/rGO

Graphene nanoplatelets provide a conductive carbon framework that can be coupled directly with $ZnFe_2O_4$ nanoparticles. A series of $ZnFe_2O_4/GNP$ nanocomposites were prepared by varying the GNP fraction. The optimized composite exhibited a specific capacitance of $314\ F\ g^{-1}\ at\ 0.5\ A\ g^{-1}$, together with 77.6% capacitance retention [13]. Electrochemical behaviour to the conducting nature of GNPs and the improved electrode/electrolyte charge-transfer interface. The graphene phase is not limited to increasing bulk conductivity. In the $ZnFe_2O_4/GNP$ system, the carbon phase creates a conductive environment around the ferrite and facilitates charge transfer at the electrode/electrolyte interface, interfacial coupling between $ZnFe_2O_4$ nanoparticles and $GNPs$, demonstrating that the quality of the ferrite-carbon interface is an important factor governing the electrochemical response [13].

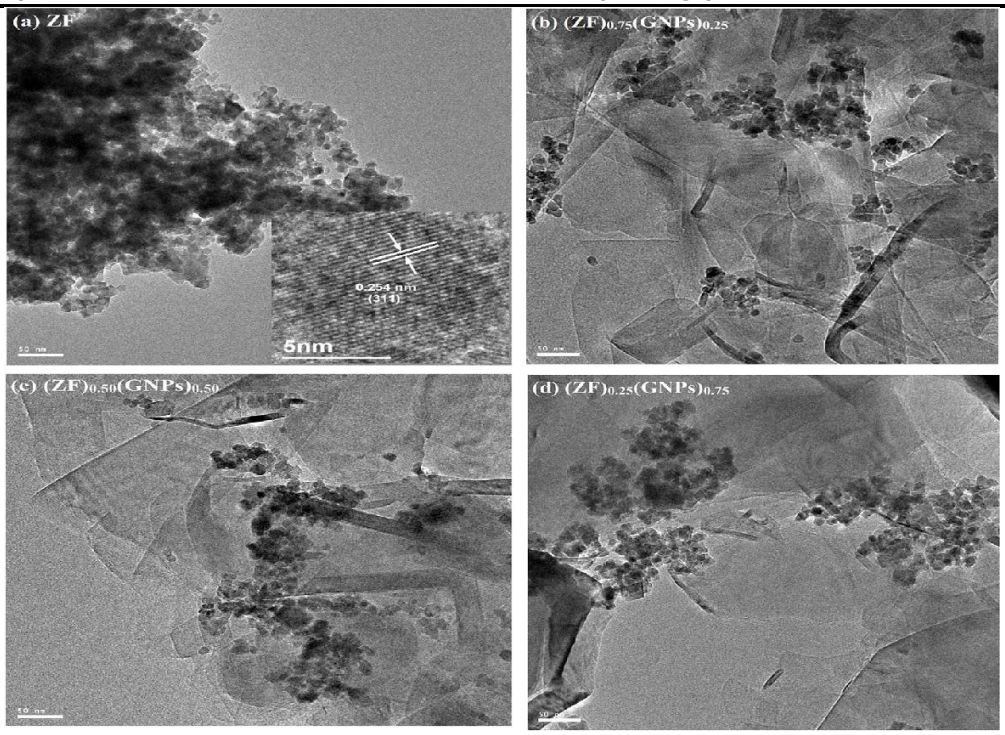


Fig. 1: $ZnFe_2O_4$/graphene morphology and interface - $ZnFe_2O_4$ nanoparticles anchored on conductive graphene [13].

Carbon architecture of $ZnFe_2O_4@C/rGO$ studies the $ZnFe_2O_4$ nanoparticles were first coated with a carbon layer and subsequently integrated with rGO nanosheets. TEM analysis showed $ZnFe_2O_4$ nanoparticles with dimensions of approximately 15-20 nm, surrounded by a continuous carbon shell of approximately 2 nm. The carbon-coated nanoparticles were further distributed over rGO sheets, producing a hierarchical architecture, XRD and HRTEM confirmed the cubic spinel $ZnFe_2O_4$ phase, while the $ZnFe_2O_4$ crystalline domains in the composite were approximately 16 nm, The interfacial chemistry of $ZnFe_2O_4$ nanoparticles were treated with polyacrylic acid, whose carboxyl groups coordinated with Zn^{2+} and Fe^{3+} at the nanoparticle surface. Subsequent interaction with graphene oxide and thermal treatment generated the $ZnFe_2O_4@C/rGO$ structure. The researchers identified $C-O-M$ interfacial linkages and associated these interactions with improved charge transfer and stronger attachment of $ZnFe_2O_4$ to the carbon framework [41].

CNTs

$CNTs$ were used as part of the conductive-agent formulation during preparation of the $ZnFe_2O_4@C/rGO$ electrode. The electrode slurry contained carbon black and $CNTs$ as conductive components. The $CNTs$ functioned as conductive additives rather than the carbon phase surrounding or anchoring $ZnFe_2O_4$ [41].

3.2 $ZnFe_2O_4/Conducting\ Polymer$ Composites

Conducting polymers are attractive components for hybrid supercapacitor electrodes because they combine electronic conductivity with reversible Faradaic charge storage. The polyaniline (PANI), polypyrrole (PPy), and PEDOT: PSS among the important conjugated conducting polymers used in electrochemical energy storage systems. In particular, PANI and PPy are described as pseudocapacitive electrode materials because of their redox activity, relatively high capacitance, adjustable electrochemical behaviour, and good electrical conductivity [31].

3.2.1 Polyaniline (PANI)

PANI is a redox-active conducting polymer whose electrochemical charge storage originates primarily from reversible oxidation/reduction of the polymer backbone. Conducting polymers such as PANI and PPy can provide relatively high capacitance and adjustable redox activity, however, repeated redox cycling can generate mechanical stress in the polymer, which may contribute to capacitance degradation during prolonged cycling. PANI-modified graphene hydrogel electrode, which delivered $530\ F\ g^{-1}$ and retained 80% of its initial capacitance after 10,000 charge-discharge cycles at $10\ A\ g^{-1}$ [31].

3.2.2 Polypyrrole (PPy)

PPy structural relationship with $B-rGO/ZnFe_2O_4/PPy$ ternary heterostructure, prepared by synthesizing the $B-rGO/ZnFe_2O_4$ hybrid and subsequently incorporating PPy through polymerization, resulting material contained $ZnFe_2O_4$ nanoparticles associated with B-doped reduced graphene oxide and a PPy phase. PPy increased the anodic and cathodic current response of the $B-rGO/ZnFe_2O_4$ system, indicating modification of its charge-transfer characteristics [22].

$Ni_{0.5}Zn_{0.5}Fe_2O_4/polyindole$ study provides a more directly relevant conducting-polymer/ferrite analogue, $Ternary\ 3D\ rGO/Ni_{0.5}Zn_{0.5}Fe_2O_4/polyindole$ (PIN) hybrid through hydrothermal synthesis followed by in-situ emulsion polymerization of polyindole, material contains $Ni_{0.5}Zn_{0.5}Fe_2O_4$ rather than pristine $ZnFe_2O_4$, it provides useful evidence for the design principle of combining a spinel ferrite with a conducting polymer and carbon framework. The ternary hybrid exhibited a specific capacitance $of\ 320\ F\ g^{-1}$ at 0.3 $A\ g^{-1}$, whereas the corresponding PIN and PIN/NZF-containing electrodes showed substantially lower values under the reported conditions. The porous ternary architecture facilitated electrolyte-ion diffusion toward electrochemically active regions, while interactions among the polymer chains, ferrite nanoparticles, and graphene framework contributed to the electrochemical response, The scan-rate analysis is particularly informative. The b value of approximately 0.81 near the cathodic peak, while values approached 1 at potentials farther from the peak, indicating that the total charge-storage response contained both diffusion-controlled Faradaic and surface-controlled capacitive contributions, the conducting-polymer/ferrite interface should not be interpreted as producing a purely pseudocapacitive response. Instead, the experimentally observed behaviour can contain surface-controlled charge storage, diffusion-controlled redox reactions, and EDLC contributions, depending on the architecture and measurement conditions [20].

3.2.3 PEDOT and Related Conducting Polymers

PEDOT/PEDOT:PSS is identified in this electrochemical energy storage literature as a member of the conjugated conducting-polymer family, together with PANI, PPy, and related polymers, PEDOT can consequently be presented as a potential conducting-polymer platform for future $ZnFe_2O_4$-based hybrid electrodes [31].

3.2.4 Electrochemical Synergy and Limitations

The fundamental attraction of $ZnFe_2O_4/conducting-polymer$ composites is the possibility of combining inorganic Faradaic activity with polymeric pseudocapacitance and improved electronic transport. EDLC materials from redox-active transition-metal compounds and conducting polymers, emphasizing that hybridization can combine physical and Faradaic charge-storage processes within one electrode [31]. For conducting polymers, however, the principal limitation is cycling-induced structural stress. Oxidation/reduction can generate mechanical deformation and eventually degrade electrochemical stability [31]. $Ni_{0.5}Zn_{0.5}Fe_2O_4/polyindole$ study provides three-dimensional rGO-supported architecture. The researchers reported that the graphene framework helped immobilize active components, provided electron-transfer pathways, and improved the structural stability of the hybrid, The same study shows that the ternary hybrid achieved 320 $F\ g^{-1}\ at$ 0.3 $A\ g^{-1}$, with the capacitance decreasing as the current density increased. The electrode retained approximately 69.6% of its capacitance when the current density increased from 0.3 to 8 $A\ g^{-1}$, corresponding asymmetric device, the reported capacitance was 48.9 F g^{-1} at 0.5 $A\ g^{-1}$, with an energy density of 16.38 $Wh\ kg^{-1}\ at$ 1784 $W\ kg^{-1}$ and approximately 84% capacitance retention after 1500 cycles [20].

3.2.5 Comparative Scientific Assessment of Material

Polymer	Scientific interpretation	Ref.
PANI	Established pseudocapacitive polymer	31
PPy	Demonstrates $ZnFe_2O_4-PPy$ integration and modified charge transfer.	22
Polyindole	Strong analogous evidence for ferrite-conducting-polymer-carbon synergy, 320 $F\ g^{-1}\ at$ 0.3 $A\ g^{-1}$	20
PEDOT/PEDOT: PSS	Potential future partner, no direct $ZnFe_2O_4/PEDOT$ performance	31

Table 1: Scientific assessment of $ZnFe_2O_4/polymer-based$ nanocomposite material

3.3 $ZnFe_2O_4/Metal\ Oxide$ Heterostructures

Heterostructure provides a distinct strategy for improving the electrochemical utilization of $ZnFe_2O_4$ by coupling it with a second redox-active oxide or ferrite phase. Unlike simple physical blending, a heterostructure creates an interface at which the two phases can interact chemically and electronically. Such an interface can modify the electroactive sites, facilitate charge redistribution, and provide additional pathways for electrolyte-ion transport. $NiFe_2O_4/ZnFe_2O_4$ asymmetric architectures and an electrochemically generated $zinc(iron)oxyhydroxide/ZnFe_2O_4$ heterostructure [16,21]. Fig. 2. show the Heterointerface engineering of $Zn(Fe)OOH/ZnFe_2O_4$ interface and evolution during cycling [21].

3.3.1 Synergistic Redox Behaviour

Spinel ferrites possess multiple transition-metal redox centres, making ferrite-ferrite combinations attractive for hybrid charge-storage architectures. $NiFe_2O_4$ nanoparticles and $ZnFe_2O_4$ nanorods were independently synthesized through an ice-crystal-assisted precipitation route. The resulting structures contained abundant voids and porous networks, which exposed electroactive regions and provided pathways for electrolyte transport, The electrochemical behaviour of the two ferrites was distinctly Faradaic. For $NiFe_2O_4$, the observed redox features were associated with $Ni^{2+}/Ni^{3+}\ and\ Fe-based$ redox processes, whereas the $ZnFe_2O_4$ electrode exhibited a corresponding Faradaic response associated with Fe-containing redox chemistry in alkaline electrolyte, The $ZnFe_2O_4$ nanorod electrode reached a specific capacity of $1005\ C\ g^{-1}$ $(1671\ F\ g^{-1})\ at\ 1\ A\ g^{-1}$, while the $NiFe_2O_4$ nanoparticle electrode delivered $1403\ C\ g^{-1}$ $(2338\ F\ g^{-1})$ under the same current density [16]. The resulting $NiFe_2O_4//ZnFe_2O_4$ device operated over a potential window of approximately 1.6 V and delivered an energy density of 99.55 $Wh\ kg^{-1}$ at 1.28 $kW\ kg^{-1}, with$ 95% capacity retention after 15,000 cycles [16].

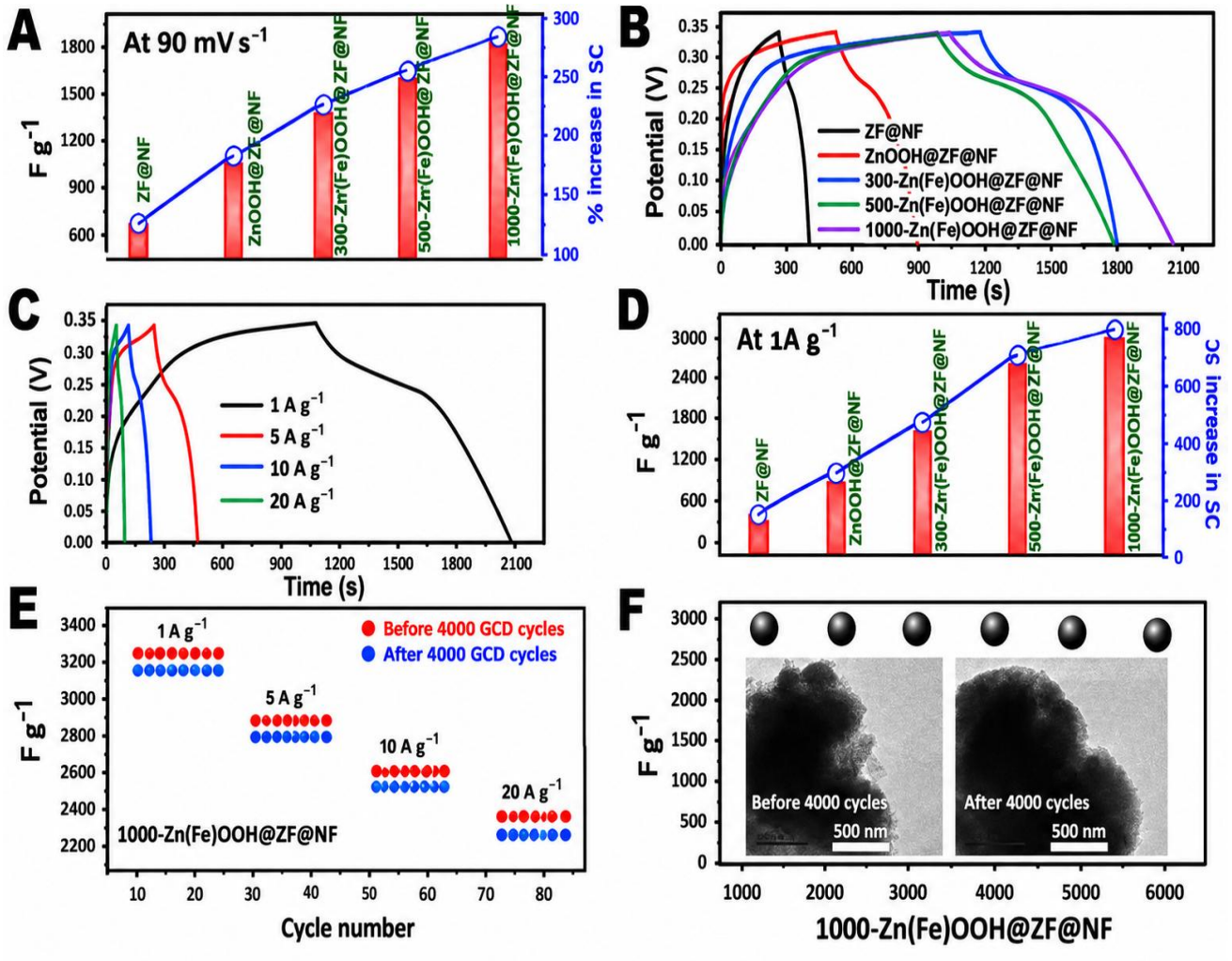


Fig. 2: Heterointerface engineering of $Zn(Fe)OOH/ZnFe_2O_4$ interface and evolution during cycling [21].

$Zinc(iron)oxyhydroxide/ZnFe_2O_4, ZnFe_2O_4$ nanosheets supported on nickel foam were subjected to repeated oxygen-evolution-reaction cycles in aqueous KOH. The outer regions of $ZnFe_2O_4$ underwent partial phase transformation, producing a $Zn(Fe)OOH/ZnFe_2O_4$ heterostructure, it forms directly from the surface of $ZnFe_2O_4$, producing an intimate phase boundary, $Zn(Fe)OOH/ZnFe_2O_4$ interface increases the

number of accessible electroactive sites and modifies the interaction of the electrode surface with hydroxide ions. Consequently, the heterostructure exhibited enhanced charge-storage behaviour as the electrochemically generated interface developed [21].

3.3.2 Heterointerface Engineering

$Zn(Fe)OOH/ZnFe_2O_4$ system, the interface was generated at the outer edges of $ZnFe_2O_4$ nanosheets during electrochemical cycling. The formation of this interface was accompanied by changes in porosity, crystallinity, hydrophilicity, and composition, the chemical and physical environment of the electrode. Strong ionic interactions at the newly formed interface increased surface hydrophilicity, while the polycrystalline oxyhydroxide phase created additional accessible regions for electrolyte interaction [21]. This observation provides an important design principle for $ZnFe_2O_4$-based heterostructures, the interface should be engineered not only for electronic coupling but also for electrolyte accessibility. A highly conductive interface that is inaccessible to electrolyte ions would not necessarily translate into effective pseudocapacitive utilization. The $NiFe_2O_4/ZnFe_2O_4$ system provides a complementary structural perspective, ferrites were synthesized as porous, void-rich nanostructures. $ZnFe_2O_4$ was obtained in nanorod form, while $NiFe_2O_4$ formed nanoparticles, the resulting morphologies contained interconnected voids that increased the available electroactive surface and facilitated electrolyte penetration. The importance of this porous architecture is also evident from impedance measurements. For the flexible $NiFe_2O_4//ZnFe_2O_4$ asymmetric device, the solution resistance and charge-transfer resistance remained low after extended cycling, with reported values changing from $0.11\ to\ 0.14\ \Omega\ and\ 0.26\ to\ 0.19\ \Omega$, respectively. The researchers associated these characteristics with rapid electrolyte-ion intercalation/deintercalation through the void-rich structures [16].

Therefore, heterointerface engineering in $ZnFe_2O_4$ −based systems should be considered a multiscale issue, involving:

- chemical interaction between the two phases,
- interfacial redox-site generation,
- surface hydrophilicity,
- pore and void architecture,
- electrolyte accessibility, and
- electron/ion transport pathways.

3.3.3 Improved Conductivity and Ion Diffusion

The pristine $ZnFe_2O_4$ has low intrinsic electronic conductivity, which restricts the utilization of its theoretical charge-storage capability, Heterostructure formation can address this limitation when the second phase establishes more favourable pathways for charge transport or modifies the interfacial electronic environment. The $Zn(Fe)OOH/ZnFe_2O_4$ system provides direct evidence for improved ion transport rather than simply electronic conductivity. Strong ionic interactions at the heterointerface increased hydrophilicity and that the resulting three-dimensional diffusion channels reduced ion-diffusion resistance [21]. The $ZnFe_2O_4$ nanorod electrode similarly benefited from its void-rich morphology. The researchers reported that the nanorod structure contained abundant pores and voids, which increased the accessible surface area and facilitated electrolyte-ion transport [16]. The resulting $ZnFe_2O_4$ electrode maintained approximately 97% capacity retention after 15,000 cycles, demonstrating that the porous architecture could simultaneously support high charge storage and long-term stability [16].

3.4 Morphology and Architecture Engineering

Morphology and electrode architecture are critical parameters governing the electrochemical utilization of $ZnFe_2O_4$ which from conventional particulate structures to nanoparticles, nanorods, nanosheets, porous assemblies, and core-shell/three-dimensional architectures can substantially alter the accessible electrochemical surface, electrolyte penetration, charge-transfer pathways, and structural stability. Importantly, these effects are not determined by particle size alone, the connectivity, porosity, orientation, and integration of the active phase with the current collector or conductive matrix also influence the resulting electrochemical response [4,13,16,21,41].

3.4.1 Nanoparticles, Nanorods, and Nanosheets

Nanoparticles provide a high density of surface and near-surface sites because decreasing the characteristic particle dimension increases the fraction of material accessible to the electrolyte. In the $ZnFe_2O_4/graphene$ nanoplatelet system, $ZnFe_2O_4$ nanoparticles were integrated with graphene nanoplatelets, and optimization of the composite composition produced a specific capacitance of $314\ F\ g^{-1}\ at\ 0.5\ A\ g^{-1}, with\ 77.6\%$ retention during cycling [13]. The researchers associated the improved electrochemical behaviour with the conducting nature of GNPs and enhanced electrode/electrolyte charge-transfer characteristics [13].

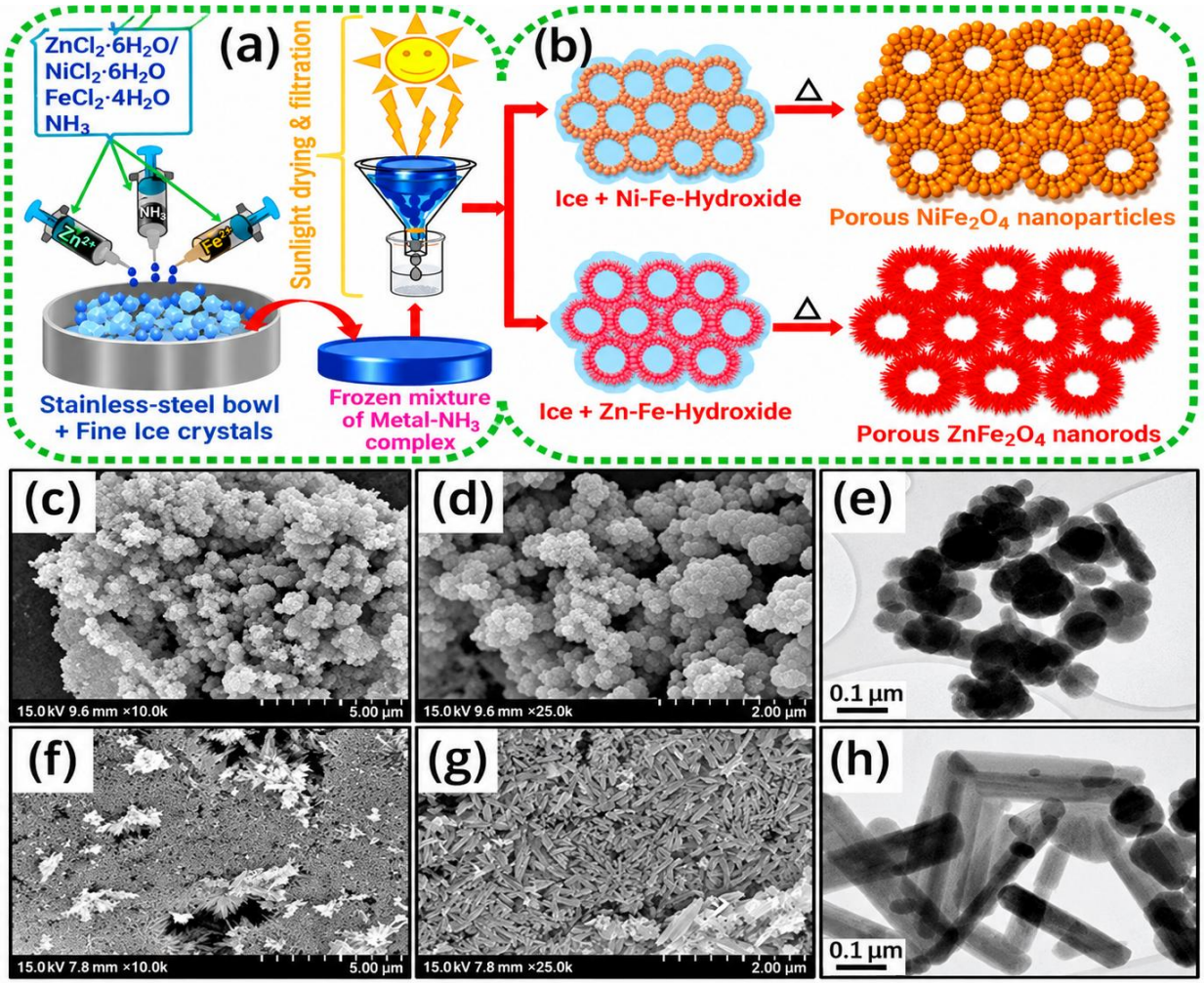


Fig. 3: $ZnFe_2O_4$ nanocomposite design concept / morphology - synthesis route and porous $ZnFe_2O_4$ nanorod architecture [16].

The effect of particle morphology is particularly evident when $ZnFe_2O_4$ is prepared as nanorods. Synthesized $ZnFe_2O_4$ nanorods through an ice-crystal-assisted precipitation process and reported that the nanorods contained abundant porous voids [16]. The resulting $ZnFe_2O_4$ NR electrode exhibited a specific capacity of $1005\ C\ g^{-1}\ at\ 1\ A\ g^{-1}$ and maintained more than 97% $capacity$ retention $after$ 15,000 $cycles$ [16]. The electrochemical behaviour to the combination of electroactive sites, multiple redox couples, porous structure, and rapid electrolyte-ion transport pathways [16]. Fig. 3: show that $ZnFe_2O_4$ nanocomposite concept / morphology - synthesis route and porous $ZnFe_2O_4$ nanorod architecture [16]. Nanosheets represent morphology because their small thickness can shorten the diffusion distance between the electrolyte and the underlying active material. $ZnFe_2O_4/nickel-foam$ study, $ZnFe_2O_4$ nanosheets were grown directly on $Ni\ foam$ through a hydrothermal process followed by calcination, before conversion to $ZnFe_2O_4$, the precursor $ZnFe-LDH$ nanosheets were approximately 71.5 nm thick and interconnected to form a porous three-dimensional flower-like structure. After calcination, conversion to spinel $ZnFe_2O_4$ reduced the nanosheet thickness to approximately 36 nm as a consequence of dehydration and structural contraction [21].

Thus, the demonstration of three useful morphological regimes,

- Nanoparticles: high surface exposure and short characteristic dimensions [13,41].
- Nanorods: anisotropic structures capable of generating interconnected voids and ion-transport pathways [16].
- Nanosheets: thin, extended active structures with reduced characteristic diffusion length and direct current-collector integration [21].

These architectures should not, however, be regarded as intrinsically superior to one another. Their electrochemical effectiveness depends on the degree of aggregation, porosity, electrical connectivity, active-material loading, and electrolyte accessibility.

3.4.2 Porous and Hierarchical Structures

The formation of porosity at multiple structural length scales is one of the most effective architectural approaches demonstrated in the this $ZnFe_2O_4$ literature. Porosity increases the electrolyte-accessible surface and can provide channels for ion transport, but excessive or poorly connected porosity may reduce the volumetric density of active material. The $ZnFe_2O_4$ nanorods has e void-rich structures simultaneously supplied electroactive regions and ion-transport pathways, The resulting $ZnFe_2O_4$ nanorod electrode achieved $1005\ C\ g^{-1}\ at\ 1\ A\ g^{-1}$ and retained more than 97% of its capacity over $15{,}000\ cycles$ [16]. $ZnFe_2O_4\ nanosheet/Ni-foam$ electrode formed thin interconnected nanosheets arranged as a porous 3D flower-like structure. Conversion to $ZnFe_2O_4$ retained the nanosheet-based architecture while reducing the sheet thickness to approximately 36 nm [21]. The combination of a nanoscale building block with a microscale three-dimensional assembly is particularly useful because it simultaneously provides

1. short local diffusion distances through the thin active nanosheets
2. interconnected voids for electrolyte penetration
3. large exposed surface regions
4. direct electrical contact with the underlying Ni foam and
5. a mechanically interconnected electrode architecture [21].

The importance of architecture rather than particle size alone is also illustrated by the electrophoretically deposited $ZnFe_2O_4$ coating studied. Although the deposited $ZnFe_2O_4$ particles remained nanoscale and the coating was relatively uniform, increasing the deposition time caused the specific capacitance to decrease substantially. The electrode deposited for 0.5 min exhibited $198\ F\ g^{-1}$, whereas the 10 min deposition produced only $17.1\ F\ g^{-1}$ [4].

3.4.3 Core-Shell and Three-Dimensional Architectures

Core-shell provides a more controlled method of integrating $ZnFe_2O_4$ with a secondary functional phase. $ZnFe_2O_4@C/rGO$ architecture, in this material, $ZnFe_2O_4$ nanoparticles with dimensions of approximately 15-20 nm were coated by a continuous carbon shell of approximately 2 nm thickness and subsequently incorporated with rGO nanosheets, the continuous carbon shell preserves the nanoscale $ZnFe_2O_4$ morphology, while the rGO sheets connect multiple carbon-coated nanoparticles into a larger conductive framework. TEM observations showed numerous $ZnFe_2O_4@C$ nanoparticles distributed over the rGO sheets, and the researchers described the combined carbon shell/rGO structure as a buffering matrix and conducting network, The interface was further strengthened through the use of polyacrylic acid (PAA). Coordination between PAA carboxyl groups and Zn^{2+}/Fe^{3+} species on the $ZnFe_2O_4$ surface generated a cross-linked precursor structure, while subsequent thermal treatment produced the carbon shell and rGO-containing architecture. The electrochemical results support the structural significance of this design. In the Li-ion half-cell, $ZnFe_2O_4@C/rGO$ maintained a lithiation capacity of $692\ mA\ h\ g^{-1}\ at\ 5\ A\ g^{-1}$, while the corresponding unmodified $ZnFe_2O_4$ and $ZnFe_2O_4$@C materials decreased to 96 and $245\ mA\ h\ g^{-1}$, respectively, under the same current density, The $ZnFe_2O_4@C/rGO$ anode also retained 98.3% of its capacity after 700 cycles at $1\ A\ g^{-1}$ [41]. It is important to emphasize that these measurements are from a Li-ion hybrid supercapacitor/battery-type anode system, not a conventional aqueous $ZnFe_2O_4$ pseudocapacitor.

3.4.4 Relationship between morphology and electrochemical accessibility

The electrophoretically deposited $ZnFe_2O_4$ electrode, increasing coating thickness reduced the fraction of active material accessible at high rates [4]. In the ice-crystal-derived $ZnFe_2O_4$ nanorods, interconnected voids promoted ion transport and supported high-capacity retention [16]. In the $ZnFe_2O_4$ nanosheet/Ni-foam architecture, direct growth and thin-sheet morphology generated a porous three-dimensional electrode structure [21]. The core-shell/rGO system provides the complementary example in which nanoscale morphology is coupled to a higher-order conductive network. The 15-20 nm $ZnFe_2O_4$ nanoparticles, 2 nm carbon shell, and rGO framework create multiple levels of structural organization [41]. Consequently, an effective $ZnFe_2O_4$ electrode architecture can be considered in terms of four coupled length scales:

Nanoscale: particle/sheet thickness determines local diffusion distance.

Mesoscale: pores and interparticle voids regulate electrolyte penetration.

Microscale: hierarchical assemblies determine connectivity and electrode utilization.

Macroscale: integration with the current collector determines overall electronic transport and mechanical integrity.

This multiscale perspective is more scientifically appropriate than correlating electrochemical performance with a single morphological parameter such as particle size or BET surface area.

3.4.5 Comparative study of structural characteristics

Architecture	Structural characteristic	Demonstrated	Ref.
Nanoparticles/GNP composite	$ZnFe_2O_4$ nanoparticles integrated with graphene nanoplatelets	314 F g^{-1} at 0.5 A g^{-1}, improved charge-transfer environment	[13]
Nanorods	$ZnFe_2O_4$ nanorods assembled into void-rich networks	1005 C g^{-1} at 1 A g^{-1}, >97% retention after 15,000 cycles	[16]
Nanosheets/3D flower-like architecture	36 nm $ZnFe_2O_4$ nanosheets directly grown on Ni foam	Porous 3D architecture and direct current-collector integration	[21]
Electrophoretic nanoparticle coating	Nanoscale $ZnFe_2O_4$ particles in deposited films	Excessive coating thickness reduced accessible capacitance	[4]
Core-shell/3D RGO architecture	15-20 nm $ZnFe_2O_4$@~2 nm C embedded in RGO	Enhanced structural stability and high-rate Li-ion storage	[41]

Table 2: Morphology-performance relationships for $ZnFe_2O_4$

Overall, Nanoparticles provide short characteristic dimensions, nanorods and nanosheets introduce anisotropic transport pathways, porous hierarchical structures improve electrolyte accessibility, and core-shell/3D architectures integrate local protection with long-range electronic connectivity [4,13,16,21,41]. For $ZnFe_2O_4 - based$ supercapacitors, the most promising architectural direction emerging from these studies is therefore the development of thin, interconnected, hierarchically porous structures with intimate current-collector contact and deliberately engineered interfaces, rather than simply increasing $ZnFe_2O_4$ loading. The evidence from the deposited-film study [4] is particularly important in this context because it shows that excessive electrode thickness can actually decrease effective electrochemical utilization, whereas the nanorod [16], nanosheet [21], and core-shell/rGO [41] studies demonstrate how controlled architecture can simultaneously address ion accessibility and structural/electronic transport.

4. Electrochemical Charge-Storage Mechanisms

The electrochemical behaviour of $ZnFe_2O_4 - based$ electrodes are governed by the interplay between non-Faradaic charge accumulation, Faradaic surface reactions, ion transport, and electron transfer through the electrode architecture. The this studies consistently show that $ZnFe_2O_4$ electrodes do not behave as ideal electrical double-layer capacitors (EDLCs), rather, their charge storage is predominantly associated with reversible Faradaic processes, while incorporation of conductive carbon or other functional phases introduces an additional capacitive contribution [4,9,13,16,20,21].

4.1 Electrical double-layer capacitance versus pseudocapacitance

EDLC and pseudocapacitive storage arise from fundamentally different processes. In an EDLC, charge is accumulated through electrostatic separation of electrolyte ions at the electrode/electrolyte interface without requiring a bulk chemical transformation. In contrast, pseudocapacitance involves rapid and reversible Faradaic charge transfer associated with surface or near-surface redox reactions. $ZnFe_2O_4/graphene$ study explicitly distinguishes these two mechanisms, identifying carbonaceous materials with interfacial charge accumulation as EDLC-type materials and transition-metal oxides such as $ZnFe_2O_4$ as pseudocapacitive materials because of their reversible Faradaic reactions [13]. For $ZnFe_2O_4$, the CV profiles generally contain distinct anodic/cathodic features rather than an ideal rectangular profile, indicating that Faradaic reactions contribute substantially to charge storage. In the $ZnFe_2O_4$ nanorod electrode, characteristic redox peaks were observed throughout the investigated scan-rate range, while the GCD curves displayed nonlinear profiles with redox plateaus, both of which are consistent with Faradaic pseudocapacitive behaviour [16]. The contribution of EDLC becomes more evident after incorporation of a conductive carbon phase. In $ZnFe_2O_4/GNP$ composites, graphene nanoplatelets provide a high-surface-area conductive component capable of supporting interfacial charge accumulation, while $ZnFe_2O_4$ contributes Faradaic charge storage. The resulting electrode therefore cannot be described adequately as a purely EDLC or purely pseudocapacitive system, instead, the overall response reflects contributions from both components [13]. A similar mixed mechanism is evident in the this $ZnFe_2O_4$ −containing ferrite/polymer/carbon system. For the $3D\ RGO/Ni_{0.5}Zn_{0.5}Fe_2O_4/polyindole$ electrode, kinetic analysis gave a b value of approximately 0.81 near the cathodic peak, while values approached unity at potentials away from the peak. The researchers therefore identified simultaneous capacitance/pseudocapacitance-controlled and diffusion-controlled redox contributions [20]. Thus, for $ZnFe_2O_4 - based$ nanocomposites, it is more scientifically appropriate to consider charge storage as a continuum of surface-controlled and diffusion-influenced processes, rather than assigning every electrode exclusively to EDLC or pseudocapacitive behaviour.

4.2 Surface redox reactions of $ZnFe_2O_4$

The Faradaic response of $ZnFe_2O_4$ is associated primarily with the participation of iron-containing redox centers and their interaction with hydroxide ions in alkaline electrolytes. For $ZnFe_2O_4$ nanorods, this study relates the reaction kinetics to the Fe^{2+}/Fe^{3+} redox couple and proposes the following overall reaction [16].

$$ZnFe_2O_4 + H_2O + OH^- \quad \rightarrow \quad ZnOOH + 2FeOOH + e^-$$

The $ZnFe_2O_4$ electrophoretic-deposition study provides complementary evidence. Redox peaks occurring between approximately -1.05 and -0.6 V were attributed to Faradaic reactions involving $M-O/M-O-OH$ species, where M represents $Zn\ or\ Fe$. The researchers further associated the pseudocapacitive response with intercalation/deintercalation involving Fe^{3+} and electrolyte K^+ at the porous electrode surface [4]. The laterally and chemically reconstructed $ZnFe_2O_4$ system in [21] provides even stronger evidence for hydroxide-mediated Faradaic storage. Both pristine $ZnFe_2O_4$ and $Zn(Fe)OOH/ZnFe_2O_4$ exhibited redox peaks, and the researchers assigned the charge-storage reaction to [21].

$$ZnFe_2O_4 + OH^- + H_2O \quad \rightarrow \quad ZnOOH + 2FeOOH + e^-$$

Importantly, interpreted as demonstrating a single isolated Zn^{2+} redox couple. The electrochemical response reflects the coupled behaviour of the ferrite lattice, surface oxyhydroxide species, electrolyte ions, and transition-metal oxidation states. Therefore, descriptions such as "$Zn^{2+}/Zn^{3+}\ redox$" should not be introduced unless directly supported by the relevant experimental characterization. This evidence more directly supports Fe^{2+}/Fe^{3+}-associated redox chemistry and hydroxide-mediated surface conversion [4,16,21].

4.3 Electron-transfer pathways within $ZnFe_2O_4$ nanocomposites

The intrinsic electronic conductivity of $ZnFe_2O_4$ is a major limitation for efficient utilization of its redox-active sites. $ZnFe_2O_4/graphene$ study explicitly identifies poor conductivity as a limitation of pristine $ZnFe_2O_4$ and demonstrates that incorporation of graphene nanoplatelets improves the electrode/electrolyte charge-transfer interface, $ZnFe_2O_4/GNP$ composite, the improved electrochemical response was associated with the conducting nature of GNPs and improved electrode/electrolyte charge transfer. The composite delivered $314\ F\ g^{-1}\ at\ 0.5\ A\ g^{-1}$, together with 77.6% capacitance retention under the reported cycling

conditions [13]. $ZnFe_2O_4/g-C_3N_4$ study provides another illustration of interfacial electron transport. Incorporation of $g-C_3N_4$ increased the current response relative to pristine $ZnFe_2O_4$. The researchers attributed the enhancement to the $ZnFe_2O_4/g-C_3N_4$ interface, which increased the number of active redox sites and created additional charge-transport pathways, At $10\,A\,g^{-1}$, the $ZnFe_2O_4/g-C_3N_4$ composite exhibited a specific capacitance of $103\,F\,g^{-1}$, compared with $66\,F\,g^{-1}\,for\,pristine\,ZnFe_2O_4$ under the same conditions [9]. The researchers associated this improvement with enhanced OH^- diffusion and the charge-transport pathway provided by the N-containing $g-C_3N_4$ framework [9]. A particularly well-defined electron-transfer architecture was reported for $ZnFe_2O_4@C/rGO$. In this system, a carbon layer surrounds $ZnFe_2O_4$ nanoparticles and the particles are subsequently connected through an rGO network. Covalent $C-O-M$ linkages between $ZnFe_2O_4$ and the carbon-containing phase were reported to promote charge transfer while simultaneously improving structural stability [41]. Consequently, the electron-transport pathway in such a nanocomposite can be conceptually represented as: This architecture reduces the dependence on electron transport through isolated $ZnFe_2O_4$ particles and can increase the fraction of electrochemically accessible active material [13,41].

4.4 Electrolyte-ion diffusion and accessibility

Electrolyte-ion transport is equally important because Faradaic reactions can occur only where electrolyte ions can reach electrochemically active sites. The electrophoretic-deposition study provides direct evidence for this kinetic limitation. At low scan rates, both the outer and inner regions of the $ZnFe_2O_4$ coating could participate in ion intercalation. As the scan rate increased, ion accessibility became progressively restricted to the outer region of the coating, causing a decrease in specific capacitance [4]. The $ZnFe_2O_4$ nanorod architecture addresses this limitation through interconnected voids. The ice-crystal-assisted synthesis generated $ZnFe_2O_4$ nanorods containing abundant porous voids, which were reported to provide electroactive sites and rapid pathways for electrolyte-ion transport [16]. The rate-dependent behaviour of these nanorods further supports the role of ion transport. The $ZnFe_2O_4$ nanorod electrode delivered approximately $1005, 910, 867, 805, 700, and\ 640\ C\ g^{-1}$ at current densities of $1, 2, 3, 5, 10, and\ 20\ A\ g^{-1}$, respectively, retaining approximately 69% of its initial capacity at 20 A g^{-1} [16].

The $Zn(Fe)OOH/ZnFe_2O_4$ interface provides even more direct evidence of the relationship between interfacial structure and ion transport. Formation of the heterointerface increased the electrochemically active surface area from $442.75\,cm^2\,for\,pristine\,ZnFe_2O_4/Ni$ foam to $1628.25\,cm^2$ after the engineered interface had developed [21]. The researchers attributed this increase to enhanced hydrophilicity and the presence of external three-dimensional diffusion channels, Electrochemical impedance measurements showed that the engineered $Zn(Fe)OOH/ZnFe_2O_4$ interface possessed lower OH^- diffusion resistance than pristine $ZnFe_2O_4$. The more hydrophilic interface and external 3D diffusion channels facilitated OH^- transport toward the active interface, this explains why the specific capacitance of the engineered electrode increased substantially. At $90\,mV\,s^{-1}, the$ 1000-cycle $Zn(Fe)OOH/ZnFe_2O_4$ electrode reached $1861.713\,F\,g^{-1}$, compared with $660.350\,F\,g^{-1}$ for the pristine $ZnFe_2O_4/Ni-foam\,electrode$ [21].

4.5 Importance of heterointerfaces in accelerating charge transfer

Heterointerfaces influence charge storage through simultaneous modification of electronic coupling, electrolyte wettability, active-site density, and ion-transport pathways. The $ZnFe_2O_4/g-C_3N_4$ system demonstrates this principle clearly: formation of the heterointerface increased the current response and was associated with enhanced charge-transport pathways and OH^- diffusion [9]. The $Zn(Fe)OOH/ZnFe_2O_4$ interface provides a more direct electrochemical example. EIS measurements showed no pronounced high-to-medium-frequency semicircle for the engineered electrode, indicating negligible electron-transfer resistance under the reported measurement conditions. More importantly, its low-frequency response indicated substantially reduced OH^- diffusion resistance relative to pristine $ZnFe_2O_4$, The interface therefore operates through more than one mechanism. Its strong ionic interactions increase surface hydrophilicity, while its external 3D channels facilitate electrolyte penetration. Simultaneously, the intimate coupling between $ZnFe_2O_4$ and $Zn(Fe)OOH$ increases the number of electrochemically accessible $ZnFe_2O_4$ sites, at $1\,A\,g^{-1}$, the GCD-derived capacitance of the optimized $Zn(Fe)OOH/ZnFe_2O_4$ electrode reached 3258.080 F g^{-1}, compared with $426.471\,F\,g^{-1}$ for the corresponding pristine $ZnFe_2O_4/Ni-foam\,electrode$ [21].

However, the same study identifies an important limitation: non-uniform transformation of $ZnFe_2O_4$ into $Zn(Fe)OOH$ can generate relatively hydrophobic regions that restrict OH^- transfer at high current

densities [21]. Thus, heterointerface engineering is not automatically beneficial, interface uniformity and controlled phase conversion are essential.

4.6 Structure-mechanism-performance relationship

$ZnFe_2O_4$ coating, poor electronic conductivity and long ion-transport distances restrict utilization of internal active regions. Consequently, the specific capacitance decreases as the scan rate increases because the electrolyte ions cannot penetrate the entire electrode rapidly enough [4]. When $ZnFe_2O_4$ is converted into a void-rich nanorod architecture, the effective ion-transport distance is reduced and the electrochemically accessible surface increases. The resulting $ZnFe_2O_4$ nanorod electrode reaches $1005\ C\ g^{-1}\ at\ 1\ A\ g^{-1}$ and retains approximately 97% of its capacity after 15,000 cycles [16]. When a conductive carbon phase is introduced, the mechanism becomes more complex. In $ZnFe_2O_4/GNP$ composites, graphene provides a conductive network and interfacial charge-transfer pathway while $ZnFe_2O_4$ supplies Faradaic activity [13]. In $ZnFe_2O_4/g-C_3N_4$, the heterointerface enhances charge transport and OH^- diffusion [9]. These systems consequently demonstrate that electronic conductivity and ion accessibility must be optimized simultaneously.

The strongest evidence comes from the engineered $Zn(Fe)OOH/ZnFe_2O_4$ interface. Increasing interfacial development increased the ECSA, reduced OH^- diffusion resistance, and increased the measured capacitance [21]. The optimized electrode reached $1861.713\ F\ g^{-1}$ in CV measurements at 90 mV s^{-1} and $3258.080\ F\ g^{-1}\ from\ GCD\ at\ 1\ A\ g^{-1}$ [21].

5. Supercapacitor Performance and Critical Comparison

The electrochemical performance of $ZnFe_2O_4-based$ electrodes cannot be represented adequately by a single parameter such as specific capacitance. The studies show that specific/areal capacitance, rate capability, energy density, power density, cycling stability, electrolyte composition, and electrode configuration are strongly interdependent. In particular, the very high capacitance values obtained in three-electrode measurements do not necessarily translate into similarly high device-level energy density because the latter depends on the complete cell configuration, operating voltage, active-material mass, and discharge kinetics [4,13,16,21]. Therefore, meaningful comparison requires careful separation of three-electrode electrode performance from two-electrode full-device performance.

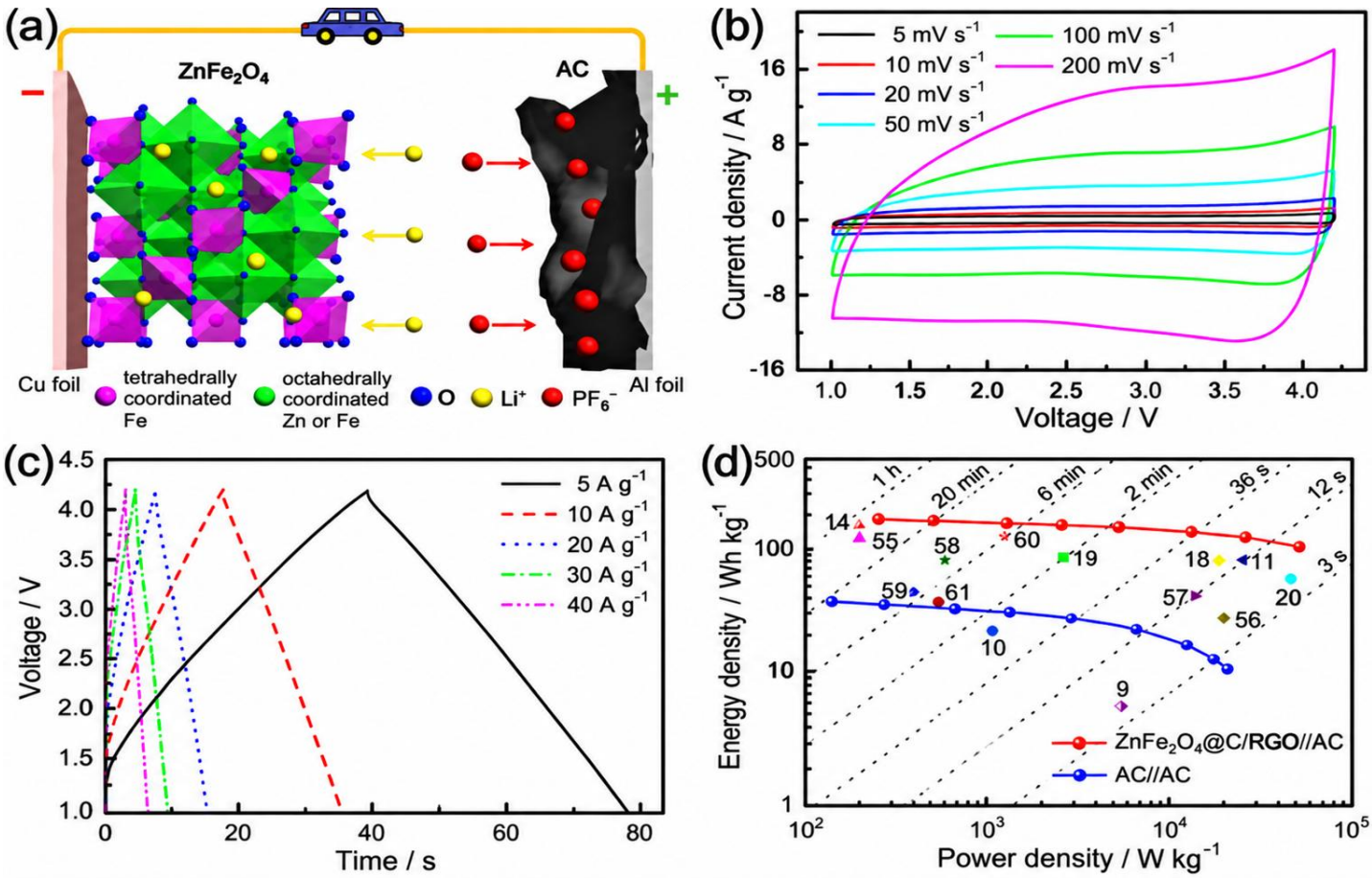


Fig.4: Li-ion hybrid supercapacitor architecture and Ragon performance.

5.1 Specific and areal capacitance

Specific capacitance is one of the most frequently reported parameters for $ZnFe_2O_4$ electrodes, but its magnitude depends strongly on the measurement configuration and normalization procedure. Deposited $ZnFe_2O_4$ study, the specific capacitance decreased from $198\ F\ g^{-1}\ to\ 17.1\ F\ g^{-1}$ when the deposition time was increased from 0.5 to 10 min. The researchers attributed this decline to the poor electrical conductivity of $ZnFe_2O_4$ and the increasing thickness of the deposited coating, which limited effective utilization of the active material [4]. This result is important because it demonstrates that increasing active-material loading does not necessarily improve the gravimetric response. A thicker electrode can introduce longer electron- and ion-transport pathways, leaving part of the deposited $ZnFe_2O_4$ electrochemically underutilized. Much higher capacitance was obtained using porous $ZnFe_2O_4$ nanorods. In the three-electrode configuration, the $ZnFe_2O_4$ nanorod electrode delivered $1005\ C\ g^{-1}$, equivalent to $1671\ F\ g^{-1}, at\ 1\ A\ g^{-1}$ and maintained more than 95% of its capacity over $15{,}000\ cycles$ [16]. The researchers related this behaviour to the void-rich porous architecture, which facilitates electrolyte-ion transport and exposes electrochemically accessible regions [16]. The strongest gravimetric response among the this aqueous $ZnFe_2O_4$ studies were reported for the electrochemically $Zn(Fe)OOH/ZnFe_2O_4/Ni-foam$ electrode. Its CV-derived specific capacitance reached $1861.713\ F\ g^{-1}\ at\ 90\ mV\ s^{-1}$, compared with 660.350 F g^{-1} for the pristine $ZnFe_2O_4$/Ni-foam electrode. From GCD measurements, the engineered electrode reached $3258.080\ F\ g^{-1}\ at\ 1\ A\ g^{-1}$, whereas the pristine electrode gave $426.471\ F\ g^{-1}$ [21].

However, these values should not be compared directly without considering the different architectures and measurement methods. The $1861.713\ F\ g^{-1}$ value is derived from CV at a specified sweep rate, whereas $3258.080\ F\ g^{-1}$ is derived from GCD. Furthermore, the latter is a three-electrode electrode measurement rather than the performance of a complete two-electrode device. The $ZnFe_2O_4/GNP$ composite provides a more moderate but useful example of conductive-carbon integration. The optimized composite exhibited $314\ F\ g^{-1}\ at\ 0.5\ A\ g^{-1}$, with the improvement attributed to enhanced electrode/electrolyte charge transfer and the conductive nature of graphene nanoplatelets [13]. $ZnFe_2O_4$/rGO exhibited 1419 F g^{-1} and approximately 93% capacitance retention after 5000 cycles [32].

These results collectively demonstrate that specific capacitance is highly sensitive to morphology, conductive-network formation, active-material loading, interfacial chemistry, electrolyte, current density, and calculation method. Fig. 4. Reveals Li-ion hybrid supercapacitor architecture and Ragone performance [41]

5.2 Energy density and power density

Energy density and power density are more meaningful at the device level because they describe how much energy a complete supercapacitor can store and how rapidly that energy can be delivered. For a conventional capacitor-type device, increasing the operating voltage has a particularly strong influence on energy storage because energy scales approximately with the square of the voltage window [16]. The importance of electrode configuration is clearly demonstrated by the flexible $NiFe_2O_4\ NP//ZnFe_2O_4\ NR$ asymmetric supercapacitor. The device employed $NiFe_2O_4$ as the positive electrode, $ZnFe_2O_4$ nanorods as the negative electrode, a cellulose separator, and $PVA-KOH$ gel electrolyte. It operated up to approximately 1.6 V and delivered an energy density of $99.55\ Wh\ kg^{-1}\ at\ 1.28\ kW\ kg^{-1}$ [16]. Importantly, the same device retained more than 50% of its energy density, corresponding to $45.51\ Wh\ kg^{-1}$, even at a much higher power density of $25.6\ kW\ kg^{-1}$ [16]. This illustrates the practical trade-off between energy and power: as discharge becomes faster, the accessible charge-storage contribution decreases. The $ZnFe_2O_4/NRG$ symmetric device provides a contrasting example. According to the comparative data reported in the this $Zn(Fe)OOH/ZnFe_2O_4$ study, the $ZnFe_2O_4//NRG$ device delivered $6.7\ Wh\ kg^{-1}\ at\ 3.0\ kW\ kg^{-1}$, with approximately 84% retention after 1000 cycles [21]. The substantial difference between this device-level energy density and the much higher values reported for the $NiFe_2O_4//ZnFe_2O_4$ asymmetric system demonstrates why electrode-level capacitance should never be equated directly with device-level energy density.

Core-shell $ZnFe_2O_4@C/rGO$ study provides an additional but chemically different example. Its Li-ion hybrid supercapacitor, employing $ZnFe_2O_4@C/rGO$ as the anode and activated carbon as the cathode, achieved $174\ Wh\ kg^{-1}\ at\ 0.25\ kw\ kg^{-1}$ and retained an energy density of $109\ Wh\ kg^{-1}\ at\ 51.4\ kw\ kg^{-1}$. This value should not be placed in the same direct performance category as aqueous $ZnFe_2O_4$ supercapacitors, because the device is a Li-ion hybrid supercapacitor with a battery-type $ZnFe_2O_4-based$ anode and activated-carbon cathode. Its higher energy density reflects, in part, the different electrochemical storage mechanism and device architecture [41].

5.3 Rate capability

Rate capability describes the ability of an electrode or device to retain charge-storage capacity as the applied current or scan rate increases. It is particularly important for $ZnFe_2O_4$ because its Faradaic reactions can be limited by both electronic transport and electrolyte-ion diffusion. The electrophoretically deposited $ZnFe_2O_4$ electrode illustrates this limitation clearly. Increasing the deposition thickness caused a pronounced reduction in specific capacitance, indicating that the internal portion of a thick $ZnFe_2O_4$ layer becomes increasingly difficult to access electrochemically [4].

By contrast, the void-rich $ZnFe_2O_4$ nanorods retained approximately 69% of their initial capacity at 20 A g^{-1}, compared with the value at 1 A g^{-1}. The reported capacity decreased from approximately $1005\ C\ g^{-1}\ at\ 1\ A\ g^{-1}$ to approximately $640\ C\ g^{-1}\ at\ 20\ A\ g^{-1}$ [16]. This behavior indicates that the porous architecture can sustain relatively rapid ion transport even under substantially increased current demand. The $Zn(Fe)OOH/ZnFe_2O_4/Ni-foam$ electrode retained approximately 72.2% of its GCD-derived capacitance at $20\ A\ g^{-1}$. The researchers attributed this rate response to the external three-dimensional percolated channels and hydrophilic interface, which facilitated ion transport during the Faradaic reaction [21]. The $ternary\ rGO/Ni_{0.5}Zn_{0.5}Fe_2O_4/polyindole$ electrode similarly exhibited a capacitance retention of 69.6% when the current density increased from 0.3 to 8 A g^{-1}. The researchers related this behaviour to improved utilization of both internal and external active regions within the hybrid architecture [20].

These results indicate that rate capability is primarily an architectural property as much as a compositional property. Shorter diffusion lengths, interconnected pores, conductive carbon frameworks, and intimate contact between active material and current collector can collectively reduce kinetic limitations.

5.4 Cycling stability

Cycling stability is essential because the high surface area and repeated Faradaic reactions of nanostructured transition-metal oxides can potentially cause structural or interfacial degradation. The void-rich $ZnFe_2O_4$ nanorod electrode exhibited particularly strong long-term stability, retaining approximately 97% of its initial capacity after 15,000 cycles in the three-electrode configuration. The corresponding $NiFe_2O_4$ electrode retained approximately 98% under the same conditions. When these materials were assembled into the flexible $NiFe_2O_4//ZnFe_2O_4$ asymmetric device, the cell retained 95% of its capacity after 15,000 GCD cycles [16]. The preservation of the Nyquist response after cycling, together with very small changes in solution, charge-transfer, and Warburg resistances, was interpreted as evidence for stable ion transport within the porous electrode structures [16]. The $Zn(Fe)OOH/ZnFe_2O_4$ electrode also demonstrated strong cycling stability. After 6000 GCD cycles at 10 A g^{-1} in $3\ M\ KOH$, the specific capacitance decreased by only approximately 2.23% [21]. This corresponds to approximately 97.8% retention. The $ZnFe_2O_4/GNP$ composite exhibited 77.6% retention under its reported cycling conditions [13]. The $ZnFe_2O_4/rGO$ system reported approximately 93% retention after 5000 cycles [32]. The ternary $rGO/Ni_{0.5}Zn_{0.5}Fe_2O_4/polyindole$ electrode maintained stable behavior over 1500 cycles, while its complete asymmetric device retained 84% capacitance after 1500 cycles [20].

These results indicate that carbon incorporation and hierarchical architectures can substantially improve cycling durability, but cycle number alone is insufficient for comparison. Current density, electrolyte, cell configuration, active-mass loading, and whether the measurement is performed on an individual electrode or complete device must also be reported.

5.5 Coulombic efficiency

Coulombic efficiency is an important indicator of charge-discharge reversibility and is defined from the ratio between discharge and charge times under equivalent current conditions. Although several these studies discuss reversibility through CV/GCD profiles and cycling behaviour, quantitative coulombic-efficiency values are not consistently reported across the $ZnFe_2O_4$. For example, the flexible $NiFe_2O_4//ZnFe_2O_4$ asymmetric device maintained highly similar charge-discharge behaviour during extended cycling, while its CV curves remained substantially unchanged even under bending conditions [16]. These observations support good electrochemical reversibility, but they should not be converted into a numerical coulombic efficiency unless that value was explicitly reported.

The issue becomes especially important when comparing different device types. In the $ZnFe_2O_4@C/rGO\ Li-HSC$, for example, the near-triangular GCD curves and small IR drop indicated favorable charge-transfer behavior, but the principal reported performance metrics were capacitance,

energy/power density, and capacity retention rather than a standalone coulombic-efficiency value [41]. Therefore, for your review, it is preferable to state "high charge–discharge reversibility" when supported by the GCD/CV behavior rather than inserting an unreported numerical coulombic efficiency.

5.6 Influence of electrolyte

Electrolyte composition strongly affects the electrochemical response because $ZnFe_2O_4$ charge storage involves surface/near-surface Faradaic reactions and electrolyte-ion transport. $ZnFe_2O_4$ coating study used 0.1 M NaOH in a three-electrode configuration with $ZnFe_2O_4$ as the working electrode, $Ag/AgCl$ as reference, and Pt as counter electrode [4]. $Zn(Fe)OOH/ZnFe_2O_4$ electrode was evaluated in 3 M KOH, where the high concentration of OH^- provided the electrolyte environment required for the reported hydroxide-mediated Faradaic reactions. The optimized electrode reached 3258.1 F g^{-1} at 1 A g^{-1} under these conditions [21]. The $NiFe_2O_4//ZnFe_2O_4$ flexible asymmetric device employed PVA–KOH gel electrolyte, enabling a solid-state architecture and an operating voltage of approximately 1.6 V [16]. In the ternary $rGO/Ni_{0.5}Zn_{0.5}Fe_2O_4/polyindole$ device, the asymmetric cell used $1\ M\ H_2SO_4$ as the electrolyte and operated to approximately 1.7 V [20].

These examples illustrate why performance values measured in different electrolytes should not be compared as though they were obtained under identical conditions. $KOH, NaOH, H_2SO_4$, and gel electrolytes differ in ionic conductivity, ion size, interfacial chemistry, accessible potential window, and interaction with the active electrode.

5.7 Influence of electrode configuration

Electrode configuration is perhaps the most important factor when comparing apparently different performance values.

Three-electrode configuration

Three-electrode measurements are useful for evaluating the intrinsic electrochemical behavior of a material because the working electrode potential can be controlled independently. Very high specific capacitance values are frequently obtained in this configuration. Examples from the this studies include:

- $ZnFe_2O_4$ nanorods: 1671 F g^{-1} at 1 A g^{-1} [16].
- $Zn(Fe)OOH/ZnFe_2O_4/Ni$ foam: 3258.1 F g^{-1} at 1 A g^{-1} [21].
- $ZnFe_2O_4/GNP$: 314 F g^{-1} at 0.5 A g^{-1} [13].
- $rGO/Ni_{0.5}Zn_{0.5}Fe_2O_4/polyindole$: 320 F g^{-1} at 0.3 A g^{-1} [20].

These values are useful for assessing material-level behaviour, but they should not be presented as equivalent to the capacitance of a complete commercial-type supercapacitor.

Two-electrode asymmetric configuration. The two-electrode asymmetric configuration provides a more realistic assessment of device operation because both positive and negative electrodes contribute to the total cell response. The flexible $NiFe_2O_4//ZnFe_2O_4$ device is a representative example, reaching 99.55 Wh kg^{-1} at 1.28 kW kg^{-1} and retaining 95% after 15,000 cycles [16].

The RGO/polyindole/ferrite asymmetric device provides another example, although the ferrite is $Ni_{0.5}Zn_{0.5}Fe_2O_4$ rather than $ZnFe_2O_4$. Its cell capacitance was $48.9\ F\ g^{-1}\ at\ 0.5\ A\ g^{-1}$, with $16.38\ Wh\ kg^{-1}\ at\ 1784\ W\ kg^{-1}$ and 84% retention after 1500 cycles [20].

Li-ion hybrid supercapacitor configuration

The $ZnFe_2O_4@C/rGO//activated-carbon\ Li-HSC$ represents a different class of device. Here, $ZnFe_2O_4$ participates in Li^+ intercalation while activated carbon stores charge through an EDLC mechanism. The complete device delivered 174 Wh kg^{-1} at 0.25 kW kg^{-1} and retained $109\ Wh\ kg^{-1}\ at\ 51.4\ kW\ kg^{-1}$ [41]. Because the underlying mechanism and electrolyte differ from those of aqueous pseudo capacitors, this system should be discussed separately rather than directly ranked against conventional aqueous $ZnFe_2O_4$ supercapacitors.

5.8 Critical Comparison $ZnFe_2O_4$ Based Composite Materials

Electrode	Electrolyte	Main capacitance	Energy density	Power density	Cycling stability	Ref.
$ZnFe_2O_4$ coating	0.1 M NaOH	198 F g^{-1} at 0.5-min deposition	-	-	-	[4]
$ZnFe_2O_4$/GNP	-	314 F g^{-1} at 0.5 A g^{-1}	-	-	77.6% retention	13
$ZnFe_2O_4$//NRG	1 M KOH	25 F g^{-1} at 1.33 A g^{-1}	6.7 Wh kg^{-1}	3.0 kW kg^{-1}	84% after 1000 cycles	21
$ZnFe_2O_4$ nanorods	KOH-based	1671 F g^{-1} at 1 A g^{-1}	-	-	>95% after 15,000 cycles	16
$NiFe_2O_4$//$ZnFe_2O_4$	PVA–KOH	-	99.55 Wh kg^{-1}	1.28 kW kg^{-1}	95% after 15,000 cycles	16
Zn(Fe)OOH/$ZnFe_2O_4$/Ni foam	3 M KOH	3258.1 F g^{-1} at 1 A g^{-1}	-	-	97.8% after 6000 cycles	21
RGO/$Ni_{0.5}Zn_{0.5}Fe_2O_4$/polyindole	1 M H_2SO_4	320 F g^{-1} at 0.3 A g^{-1}	-	-	stable to 1500 cycles	20
RGO/$Ni_{0.5}Zn_{0.5}Fe_2O_4$/polyindole ASC	1 M H_2SO_4	48.9 F g^{-1} at 0.5 A g^{-1}	16.38 Wh kg^{-1}	1.784 kW kg^{-1}	84% after 1500 cycles	20
$ZnFe_2O_4$@C/RGO //AC Li-HSC	Li-ion electrolyte	78 F g^{-1} device capacitance	174 Wh kg^{-1}	0.25 kW kg^{-1}, 109 Wh kg^{-1} at 51.4 kW kg^{-1}	80.5% after 10,000 cycles	41

Table 3: comparative study of electrochemical studies of $ZnFe_2O_4$-based nanocomposites

The values in this table should be interpreted within their respective experimental configurations, rather than as a universal performance ranking. In particular, three-electrode specific capacitance, two-electrode device capacitance, and Li-ion hybrid-device performance represent different levels of evaluation.

6. Challenges, Research Gaps and Future Perspectives

Despite the substantial progress demonstrated by the this studies, several issues continue to limit the transition of $ZnFe_2O_4 - based$ nanocomposites from laboratory-scale electrode materials to practically relevant supercapacitor technologies. The major challenges are not restricted to increasing specific capacitance, rather, they involve electronic transport, structural durability, electrode-scale utilization, synthesis reproducibility, mechanistic understanding, and device-level validation. The following issues emerge directly from this literature.

6.1 Limited Intrinsic Electrical Conductivity

The intrinsically limited electronic conductivity of $ZnFe_2O_4$ remains one of the fundamental barriers to efficient utilization of its redox-active sites. The this heterostructure study explicitly identifies low intrinsic electronic conductivity and limited stability as two major factors restricting the electrochemical performance of $ZnFe_2O_4$ [21]. This limitation becomes particularly important when the active material is deposited as a relatively thick layer. In the this $ZnFe_2O_4$ electrode study, increasing the deposited amount did not improve capacitance proportionally, instead, thicker coatings showed reduced electrochemical utilization, indicating limitations in charge transport through the electrode [4]. The problem is therefore fundamentally architectural: increasing $ZnFe_2O_4$ loading without simultaneously constructing efficient electronic pathways can make a larger fraction of the active phase electrochemically inaccessible. The composite studies demonstrate several approaches to mitigating this problem. Graphene-derived phases, $g - C_3N_4$, and rGO provide electrically conductive pathways, while direct growth on conductive substrates can reduce the number of resistive interfaces. Particularly instructive is the $ZnFe_2O_4@C/rGO$ architecture, where $C - O - M$ bonding creates intimate contact between $ZnFe_2O_4$ and the carbon framework and was reported to facilitate electron transfer [41].

Future research should therefore focus not simply on adding more conductive carbon, but on minimizing interfacial resistance while maintaining a high fraction of electrochemically active $ZnFe_2O_4$. Excessive conductive additives can increase inactive mass and may reduce the practical advantage of the high-capacity ferrite phase.

6.2 Stability and Structural Degradation During Long-Term Cycling

Long-term stability is another important consideration because $ZnFe_2O_4$ electrodes undergo repeated interfacial redox reactions and structural changes during operation. The this studies demonstrate that appropriate structural engineering can substantially improve durability, but they also reveal that stability is closely coupled to morphology and interfacial chemistry. $ZnFe_2O_4$ nanorod electrode retained approximately 97% of its initial capacity after 15,000 cycles, which was associated with the interconnected nanorod morphology, abundant voids, and high accessible surface area [16].

Similarly, the electrochemically engineered $Zn(Fe)OOH/ZnFe_2O_4$ interface developed through controlled cycling produced a polycrystalline oxyhydroxide layer with strong interfacial interactions. The researchers reported that this interface improved electrochemical stability while simultaneously increasing electroactive surface area and reducing ion-diffusion resistance [21]. However, structural modification must itself be carefully controlled. $ZnFe_2O_4/g-C_3N_4$ study demonstrates that degradation of the $g-C_3N_4$ component caused increased $ZnFe_2O_4$ agglomeration and poorer electrochemical stability during repeated cycling [3]. Thus, a composite can only provide long-term protection if its individual constituents and interfaces remain chemically and mechanically stable under operating conditions. Future studies should therefore combine post-cycling structural characterization with electrochemical analysis rather than evaluating stability exclusively through capacitance retention. SEM/TEM, XPS, Raman spectroscopy, XRD and EIS before and after cycling can help determine whether capacitance loss originates from phase transformation, particle aggregation, interface delamination, pore blockage, or changes in charge-transfer resistance.

6.3 Difficulty in Translating Three-Electrode Results into Practical Devices

One of the most important limitations in the $ZnFe_2O_4$ literature is the difference between material-level performance measured in three-electrode cells and actual device-level performance obtained in two-electrode configurations.

Several these studies report very high $ZnFe_2O_4$ electrode capacitances in three-electrode systems. For example, $ZnFe_2O_4$ nanorods exhibited $1005\ C\ g^{-1}$ $(1671\ F\ g^{-1})$ $at\ 1\ A\ g^{-1}\ in\ 6\ M\ KOH$ [16]. Asymmetric configuration using $NiFe_2O_4$ as the positive electrode and $ZnFe_2O_4$ as the negative electrode to construct a practical solid-state device [16]. This distinction is crucial because the performance of a complete device is affected by electrode mass balance, separator resistance, electrolyte configuration, voltage window, current collectors, inactive components, and the electrochemical limitations of both electrodes. The $ZnFe_2O_4$ nanorod electrode was evaluated using a three-electrode configuration, whereas the final device employed a PVA-KOH gel electrolyte, cellulose separator, $NiFe_2O_4$ positive electrode, and $ZnFe_2O_4$ negative electrode [16]. The resulting flexible device operated to approximately 1.6 V and delivered 99.55 Wh kg^{-1} at 1.28 kW kg^{-1}, while maintaining 95% capacity retention after 15,000 cycles [16]. Consequently, future $ZnFe_2O_4$ studies should place greater emphasis on two-electrode device validation rather than relying exclusively on optimized three-electrode values.

6.4 Reproducibility and Scalable Synthesis

Synthesis reproducibility is closely connected to morphology because $ZnFe_2O_4$ electrochemical behaviour depends strongly on particle size, porosity, aggregation state, and architecture. This literature shows that conventional preparation methods such as chemical-bath deposition, SILAR, coprecipitation, and dip coating can require relatively long reaction times, while variations in reaction temperature may lead to nonuniform or agglomerated nanostructures. This issue becomes particularly significant for nanocomposites because increasing the number of synthesis steps can increase batch-to-batch variation in composition and interfacial structure. The precipitation step occurred in approximately 20 min, followed by annealing, and produced self-assembled porous $ZnFe_2O_4$ nanorods. The researchers specifically described the approach as rapid, inexpensive and scalable [16]. Nevertheless, demonstration of a rapid laboratory synthesis is not equivalent to industrial scalability. Future work should establish:

- batch-to-batch reproducibility
- morphology uniformity over larger electrode areas
- precursor utilization efficiency
- energy consumption during thermal treatment,

- control of active-material loading
- solvent and waste requirements
- preservation of electrochemical performance after scale-up.

Thus, scalability should be demonstrated experimentally rather than inferred solely from a short synthesis time.

6.5 Need for Higher Mass Loading and Realistic Electrode Thickness

A major gap between laboratory demonstrations and practical electrodes is the relatively low active-material loading frequently used in electrochemical testing 1.4 mg of $ZnFe_2O_4$ nanorods on a $1 \times 1\ cm^2$ carbon-cloth current collector, such low loading facilitates efficient electrolyte penetration and minimizes electronic and ionic transport limitations. However, practical electrodes generally require substantially greater active-material loading while retaining acceptable rate capability [16]. The importance of this issue is illustrated by the dependence of performance on electrode thickness. Increasing $ZnFe_2O_4$ loading without preserving efficient transport pathways can produce a progressively underutilized interior region. Consequently, simply increasing the mass of $ZnFe_2O_4$ is unlikely to produce a proportional increase in device-level energy storage.

Future work should therefore report areal capacitance/capacity together with gravimetric values, as well as active-material loading, electrode thickness, electrode density, and full-cell mass. The use of realistic thicknesses and higher mass loading would provide a more meaningful assessment of whether a $ZnFe_2O_4$ architecture can retain its electrochemical advantages beyond the thin-electrode regime.

6.6 Better Understanding of $ZnFe_2O_4$ Redox Mechanisms

The exact charge-storage mechanism of $ZnFe_2O_4$ requires further clarification. This studies associate its electrochemical response with Fe^{2+}/Fe^{3+} chemistry and hydroxide-mediated reactions, while interfacial transformation can produce $Zn(Fe)OOH$ phases during electrochemical activation [16,21]. For example, the $ZnFe_2O_4$ nanorod study relates the redox behavior to Fe^{2+}/Fe^{3+} couples and proposes hydroxide-associated conversion between $ZnFe_2O_4\ and\ ZnOOH/FeOOH$ species [16]. $Zn(Fe)OOH/ZnFe_2O_4$ study provides particularly important evidence that the active electrode may evolve during electrochemical operation. During cycling, the edges of $ZnFe_2O_4$ partially transformed into a zinc(iron) oxyhydroxide film, producing an interface with different hydrophilicity, porosity and ion accessibility [21]. Therefore, the assumption that the pristine $ZnFe_2O_4$ crystal structure remains completely unchanged during electrochemical operation may be oversimplified. Future mechanistic investigations should combine operando/in situ XRD, XAS, Raman spectroscopy, XPS, Mössbauer spectroscopy and electrochemical kinetic analysis to distinguish:

1. surface redox from bulk transformation
2. Fe-centered redox from Zn-related processes
3. reversible oxyhydroxide formation from irreversible phase transformation
4. surface-controlled capacitance from diffusion-controlled storage
5. genuine pseudocapacitive behaviour from battery-type Faradaic reactions.

Such clarification would allow more accurate structure-mechanism-performance correlations.

6.7 Development of Flexible and Solid-State $ZnFe_2O_4$ Supercapacitors

$ZnFe_2O_4$ can participate in flexible and solid-state devices. The $ZnFe_2O_4$ nanorod study fabricated a flexible asymmetric supercapacitor using $ZnFe_2O_4$ nanorods, $NiFe_2O_4$ nanoparticles and PVA-KOH gel electrolyte, The device maintained its electrochemical characteristics under mechanical deformation and delivered a relatively high energy density while retaining 95% capacity after 15,000 cycles [16]. This establishes a useful proof of concept for flexible $ZnFe_2O_4 - containing$ systems. Direct growth of $ZnFe_2O_4$ on conductive flexible substrates and integration with gel or polymer electrolytes may therefore be preferable to mechanically fragile powder coatings. The goal should be to develop architectures in which the current collector, active material and electrolyte function as an integrated mechanically compliant electrode.

6.8 Computational and Materials-Engineering Approaches for Rational Interface Design

$ZnFe_2O_4$ and a secondary phase can be as important as the bulk composition itself. In the $ZnFe_2O_4@C/rGO$ system, deliberate interfacial bonding through $C-O-M$ linkages were used to improve electron transfer and suppress detachment of $ZnFe_2O_4$ from the carbon framework [41]. Similarly, the $Zn(Fe)OOH/ZnFe_2O_4$ system demonstrates that controlling interfacial microstructure and hydrophilicity can alter electroactive surface area and ion-diffusion resistance [21]. The $ZnFe_2O_4/g-C_3N_4$ study also describes the composite as a rationally designed heterostructure in which the interface contributes to enhanced ion diffusion and redox-site accessibility [9].

6.9 Future Research Priorities

$ZnFe_2O_4$ supercapacitor research should move from capacitance maximization toward integrated electrode and device engineering. Several priorities can be identified: First, intrinsic electronic limitations must be addressed through conductive architectures that introduce minimal inactive mass. Second, hierarchical structures should be designed to maintain ion accessibility even at substantially higher mass loading and realistic electrode thickness. Third, long-term cycling should be accompanied by post-mortem and, preferably, operando structural analysis to identify the actual origin of performance degradation or activation. Fourth, two-electrode devices should become a standard component of performance evaluation rather than an optional extension of three-electrode testing. Fifth, synthesis protocols should be evaluated for reproducibility, scale-up, energy consumption and morphological consistency. The rapid ice-crystal-assisted route provides one promising example of how synthesis time and structural control can be addressed simultaneously [16].

Finally, interface engineering should be combined with quantitative mechanistic studies and, where appropriate, computational modelling. The $ZnFe_2O_4@C/rGO$ and $Zn(Fe)OOH/ZnFe_2O_4$ systems demonstrate that controlling interfacial bonding, hydrophilicity and microstructure can simultaneously influence electron transport, ion accessibility and structural stability [21,41].

7. Conclusions

Zinc ferrite ($ZnFe_2O_4$) represents a promising redox-active material for advanced supercapacitor electrodes, but its practical electrochemical utilization is strongly constrained by its relatively limited intrinsic electronic conductivity, ion-transport limitations, and incomplete accessibility of active sites. The research discussed throughout this review demonstrates that nanocomposite engineering provides an effective strategy for overcoming these limitations by coupling $ZnFe_2O_4$ with electrically conductive, ion-accessible, and structurally stabilizing components. In particular, incorporation of conductive carbon frameworks and other functional phases can establish continuous electron-transport pathways while simultaneously improving the interfacial contact between $ZnFe_2O_4$ and the electrolyte. Morphological and architectural engineering-such as the development of porous, hierarchical, nanorod, core-shell, and three-dimensional structures-further increases the fraction of electrochemically accessible active material and reduces the characteristic distances for electrolyte-ion transport. Heterointerface engineering provides an additional degree of control by modifying interfacial charge transfer, surface chemistry, wettability, and redox-site accessibility. Consequently, the electrochemical performance of $ZnFe_2O_4$ nanocomposites should be understood as the result of cooperative interactions among composition, morphology, interface structure, electronic conductivity, and electrolyte transport, rather than as a consequence of $ZnFe_2O_4$ composition alone.

A central design principle emerging from the reviewed studies is the need to simultaneously optimize conductive networks, accessible redox-active sites, and coupled ion/electron transport pathways. A highly conductive matrix is ineffective if the $ZnFe_2O_4$ active phase remains inaccessible to electrolyte ions, while a highly porous structure may provide limited practical benefit if electronic transport between the active sites and current collector is inefficient. Similarly, increasing active-material loading without maintaining interconnected transport pathways can lead to underutilization of the electrode interior. Therefore, future electrode architectures should seek an optimized balance between active-material loading, electronic percolation, electrolyte accessibility, interfacial charge transfer, and structural integrity.

The available results also indicate that future progress should be evaluated increasingly at the device level, rather than solely through high specific-capacitance values obtained from three-electrode measurements. Realistic mass loading, electrode thickness, two-electrode configurations, long-term cycling, flexible/solid-state operation, and reproducible scalable synthesis are essential for determining the practical relevance of

$ZnFe_2O_4$ nanocomposites. At the same time, deeper mechanistic investigations are required to clarify the evolution of $ZnFe_2O_4$ and its interfaces during repeated Faradaic cycling.

Acknowledgements

The authors gratefully acknowledge the financial support provided by Rayat Shikshan Sanstha's Dada Patil Mahavidyalaya, Karjat, under the Seed Money Research Project **(Award Letter No. 452/2025–26).** The authors also sincerely thank the institution for its continuous encouragement and support.

References

1. Ismail, F. M., Ramadan, M., Abdellah, A. M., Ismail, I., Allam, N. K. Mesoporous Spinel Manganese Zinc Ferrite for High-Performance Supercapacitors. Journal of Electroanalytical Chemistry 2018.https://doi.org/10.1016/j.jelechem.2018.04.002
2. Rani, B. J., Ravi, G., Yuvakkumar, R., Ganesh, V., Ravichandran, S., Thambidurai, M., Rajalakshmi, A. P., Sakunthala, A. Pure and Cobalt-Substituted Zinc-Ferrite Magnetic Ceramics for Supercapacitor Applications. Applied Physics A 2018, 124, 511. https://doi.org/10.1007/s00339-018-1936-3
3. Joshi, B., Samuel, E., Kim, T.G., Park, C.W., Kim, Y.I., Swihart, M. T., Yoon, W. Y., Yoon, S. S. Supersonically Spray-Coated Zinc Ferrite/Graphitic-Carbon Nitride Composite as a Stable High-Capacity Anode Material for Lithium-Ion Batteries. Journal of Alloys and Compounds 2018. https://doi.org/10.1016/j.jallcom.2018.07.027.
4. Zhang, D., Li, W., Ye, R., Guo, X., Wang, S., Wang, X., Xiang, Q. A Facile Strategy for $ZnFe_2O_4$ Coating Preparing by Electrophoretic Deposition and Its Supercapacitor Performances. Journal of Materials Science: Materials in Electronics 2018, 29, 5454-5458. https://doi.org/10.1007/s10854-017-8512-z.
5. Park, J.W. et al. Orchestrated Effects of Two-Step Quenching and Sn Diffusion for Photoelectrochemical Water Splitting. Solar Energy Materials and Solar Cells 2018, 187, 207–218. https://doi.org/10.1016/j.solmat.2018.08.007.
6. Aparna, M. L., Grace, A. N., Sathyanarayanan, P., Sahu, N. K. A Comparative Study on the Supercapacitive Behaviour of Solvothermally Prepared Metal Ferrite (MFe_2O_4, M = Fe, Co, Ni, Mn, Cu, Zn) Nanoassemblies. Journal of Alloys and Compounds 2018. https://doi.org/10.1016/j.jallcom.2018.02.127
7. Mahmood, M., Yousuf, M. A., Baig, M. M., Imran, M., Suleman, M., Shahid, M., Khan, M. A., Warsi, M. F. Spinel Ferrite Magnetic Nanostructures at the Surface of Graphene Sheets for Visible Light Photocatalysis Applications. Physica B: Physics of Condensed Matter 2018. https://doi.org/10.1016/j.physb.2018.08.043
8. Nivetha, R., & Grace, A. N. (2019). Manganese and zinc ferrite based graphene nanocomposites for electrochemical hydrogen evolution reaction. Journal of Alloys and Compounds, 796, 185–195. https://doi.org/10.1016/j.jallcom.2019.05.021
9. Palanivel, B., Mudisoodum Perumal, S. D., Maiyalagan, T., Jayarman, V., Ayyappan, C., & Alagiri, M. (2019). Rational design of $ZnFe_2O_4$/g-C_3N_4 nanocomposite for enhanced photo-Fenton reaction and supercapacitor performance. Applied Surface Science, 498, 143807. https://doi.org/10.1016/j.apsusc.2019.143807
10. Ma, H., Mahadik, M. A., Kim, S. R., Wang, M., Ryu, H. I., Chung, H. S., Chae, W. S., Park, H., Jang, J. S. Surface Passivation of Zinc Ferrite Nanorod Photoanodes by Spray-Deposited Silicon Oxide Layer for Enhanced Solar Water Splitting. Journal of the Taiwan Institute of Chemical Engineers 2020, 107, 89-97, https://doi.org/10.1016/j.jtice.2019.11.014
11. Chen, T.W., Rajaji, U., Chen, S.M., Al Mogren, M. M., Hochlaf, M., Al Harbi, S. D. A., Ramalingam, R. J. A Novel Nanocomposite with Superior Electrocatalytic Activity: A Magnetic Property Based $ZnFe_2O_4$ Nanocubes Embellished with Reduced Graphene Oxide by Facile Ultrasonic Approach. Ultrasonics Sonochemistry 2019, 57, 116–124. https://doi.org/10.1016/j.ultsonch.2019.05.007
12. Elgendy, A., El Basiony, N. M., El-Taib Heakal, F., Elkholy, A. E. Mesoporous Ni-Zn-Fe Layered Double Hydroxide as an Efficient Binder-Free Electrode Active Material for High-Performance Supercapacitors. Journal of Power Sources 2020, 466, 228294. https://doi.org/10.1016/j.jpowsour.2020.228294
13. Israr, M., Iqbal, J., Arshad, A., Aisida, S. O., Ahmad, I. A Unique $ZnFe_2O_4$/Graphene Nanoplatelets Nanocomposite for Electrochemical Energy Storage and Efficient Visible Light Driven Catalysis for the Degradation of Organic Noxious in Wastewater. Journal of Physics and Chemistry of Solids 2020, 140, 109333. https://doi.org/10.1016/j.jpcs.2020.109333

14. Kim, S., Mahadik, M. A., Chae, W.-S., Ryu, J., Choi, S. H., Jang, J. S. Synthesis of Transparent Zr-Doped $ZnFe_2O_4$ Nanocorals Photoanode and Its Surface Modification via Al_2O_3/Co–Pi for Efficient Solar Water Splitting. Applied Surface Science 2020, 513, 145528. https://doi.org/10.1016/j.apsusc.2020.145528
15. Bandgar, S. B., Vadiyar, M. M., Jambhale, C. L., Kim, J.-H., Kolekar, S. S. Superfast Ice Crystal-Assisted Synthesis of $NiFe_2O_4$ and $ZnFe_2O_4$ Nanostructures for Flexible High-Energy Density Asymmetric Supercapacitors. Journal of Alloys and Compounds 2021, 853, 157129. https://doi.org/10.1016/j.jallcom.2020.157129
16. Zayani, W., Azizi, S., El-Nasser, K. S., Ali, I. O., Molière, M., Fenineche, N., Mathlouthi, H., Lamloumi, J. Electrochemical Behavior of a Spinel Zinc Ferrite Alloy Obtained by a Simple Sol-Gel Route for Ni-MH Battery Applications. International Journal of Energy Research 2020, 1-13. https://doi.org/10.1002/er.6140
17. Momeni, M. M., Najafi, M. Structural, Morphological, Optical and Photoelectrochemical Properties of $ZnFe_2O_4$ Thin Films Grown via an Electrodeposition Method. Inorganic Chemistry Communications 2021, 132, 108809. https://doi.org/10.1016/j.inoche.2021.108809 .
18. Draz, M. A., El-Maghrabi, H. H., Soliman, F. S., Selim, H., Abdel Razik, A., Amin, A. E.-s., Moustafa, Y. M., Hamdy, A., Nada, A. A. Large Scale Hybrid Magnetic $ZnFe_2O_4/TiO_2$ Nanocomposite with Highly Photocatalytic Activity for Water Splitting. Journal of Nanoparticle Research 2021, 23, 10. https://doi.org/10.1007/s11051-020-05122-z .
19. Thadathil, A., Ismail, Y. A., Periyat, P. Ternary 3D Reduced Graphene Oxide/$Ni_{0.5}Zn_{0.5}Fe_2O_4$/Polyindole Nanocomposite for Supercapacitor Electrode Application. RSC Advances 2021, 11, 35828–35841. https://doi.org/10.1039/D1RA04946A.
20. Appiah-Ntiamoah, R., Kim, H. Electrochemically Engineered Zinc(Iron)Oxyhydroxide/Zinc Ferrite Heterostructure with Interfacial Microstructure and Hydrophilicity Ideal for Supercapacitors. Journal of Colloid and Interface Science 2022, 606, 607-617. https://doi.org/10.1016/j.jcis.2021.08.053
21. Das, K. K., Paramanik, L., & Parida, K. (2021). An insight to band-bending mechanism of polypyrrole sensitized B-rGO/$ZnFe_2O_4$ p-n heterostructure with dynamic charge transfer for photocatalytic applications. International Journal of Hydrogen Energy, 46(48), 24484-24500. https://doi.org/10.1016/j.ijhydene.2021.05.019
22. Dippong, T., Levei, E.-A., Toloman, D., Barbu-Tudoran, L., & Cadar, O. (2021). Investigation on the formation, structural and photocatalytic properties of mixed Mn-Zn ferrites nanoparticles embedded in SiO_2 matrix. Journal of Analytical and Applied Pyrolysis, 158, 105281. https://doi.org/10.1016/j.jaap.2021.105281
23. Malima, N. M., Khan, M. D., Choi, J., Gupta, R. K., & Revaprasadu, N. (2023). Alloying normal and inverse spinel (Zn–Co ferrite) nanostructures via direct precursor pyrolysis for enhanced supercapacitance and water splitting. Materials Chemistry and Physics, 302, 127770. https://doi.org/10.1016/j.matchemphys.2023.127770
24. Chung, P.H., Kuo, C.T., Wang, T.H., Lu, Y.Y., Liu, C.I., Yew, T.R. A Sensitive Visible Light Photodetector Using Cobalt-Doped Zinc Ferrite Oxide Thin Films. ACS Applied Materials & Interfaces 2021, 13, 6411–6420. https://doi.org/10.1021/acsami.0c20487.
25. Santiago-Cuevas, A.J., Palacios-Cabrera, C.B., Tecuapa-Flores, E. D., Bazany-Rodríguez, I. J., Narayanan, J., Padilla-Martínez, I. I., Aguilar, C. A., Thangarasu, P. CO_2 Adsorption by Carbon Quantum Dots/Metal Ferrites (M = Co^{2+}, Ni^{2+}, and Zn^{2+}): Electrochemical and Theoretical Studies. ACS Omega 2025. https://doi.org/10.1021/acsomega.4c10723.
26. Yao, H., Ning, X., Zhao, H., Hao, A., Ismail, M. Effect of Gd-Doping on Structural, Optical, and Magnetic Properties of $NiFe_2O_4$ As-Prepared Thin Films via Facile Sol-Gel Approach. ACS Omega 2021, 6, 6305–6311. https://doi.org/10.1021/acsomega.0c06097.
27. Saini, S., Yadav, K. L., Shah, J., & Kotnala, R. K. (2022). Effect of Li^+, Mg^{2+}, and Al^{3+} substitution on the performance of nickel ferrite-based hydroelectric cells. Energy & Fuels, 36(13), 7121–7129. https://doi.org/10.1021/acs.energyfuels.2c01244
28. Liu, L., Zhang, X., Liu, Y., Gong, X. Electrochemical Energy Storage Devices: Batteries, Supercapacitors, and Battery–Supercapacitor Hybrid Devices. ACS Applied Electronic Materials 2025, 7, 2233–2270. https://doi.org/10.1021/acsaelm.5c00069.
29. Tomy, M., Rajappan, A. A., VM, V., Suryabai, X. T. Emergence of Novel 2D Materials for High-Performance Supercapacitor Electrode Applications: A Brief Review. Energy & Fuels 2021, 35, 19881–19900. https://doi.org/10.1021/acs.energyfuels.1c02743.

30. Makkar, P., Ghosh, N. N. Facile Synthesis of $MnFe_2O_4$ Hollow Sphere-Reduced Graphene Oxide Nanocomposites as Electrode Materials for All-Solid-State Flexible High-Performance Asymmetric Supercapacitors. ACS Applied Energy Materials 2020, 3, 2653–2664. https://doi.org/10.1021/acsaem.9b02360.
31. Formation of a Nanostructured Samarium-Doped Ceria-Lanthanum Strontium Cobalt Ferrite Functional Composite Cathode/Current Collector Single Layer for High-Performance SOFCs. ACS Applied Energy Materials 2025, 8, 16002–16011. https://doi.org/10.1021/acsaem.5c02506.
32. Xu, Y., Zhou, H. et al. Intrinsic Pseudocapacitive Affinity in Manganese Spinel Ferrite Nanospheres for High-Performance Selective Capacitive Removal of Ca^{2+} and Mg^{2+}. ACS Applied Materials & Interfaces 2021, 13, 38886–38896. https://doi.org/10.1021/acsami.1c09996.
33. Amarnath, P., Madhu, R. et al. Phase-Pure High-Entropy Spinel Oxide $(Ni,Fe,Mn,Cu,Zn)_3O_4$ via Thermal Plasma: A Promising Electrocatalyst for Oxygen Evolution Reaction. ACS Applied Energy Materials 2023, 6, 5899–5911. https://doi.org/10.1021/acsaem.3c00311.
34. Dhavale, R. P., Parale, V. G., Teli, A. M., Gupta, N. K., Patil, U. M., Choi, H., Patil, A. M., Phadtare, V. D., Ransing, A. A., Park, H. H. Reduced-Graphene-Oxide/Sodium-Manganese-Oxide Nanowire Nanocomposite Aerogels for Asymmetric Supercapacitors: Impact of NMO Loading. ACS Applied Materials & Interfaces 2025, 17, 25193–25205. https://doi.org/10.1021/acsami.4c22065.
35. Bhasin, I., Choudhari, G. I., Dhongde, V., Basu, S., Gedam, R. S., Subohi, O. Role of Cathode Material GDC with B-Site-Substituted $Bi_{0.5}Sr_{0.5}Fe_{0.9}X_{0.1}O_3$–ð (X = Nb, Sn, and Sb) Composites in Enhanced Electrochemical Performance of IT-SOFCs. ACS Applied Energy Materials 2025, 8, 16165–16178. https://doi.org/10.1021/acsaem.5c02610.
36. Huang, C., Qiu, X., Feng, G., Hua, Z., Xu, K., Li, B., Jiang, F., Cao, H., Li, H., Liu, Y., Xu, Y., & Zhu, Y. Three-dimensional graphene aerogel encapsulated $NiCo_2O_4$ sea urchin-like nanospheres for supercapacitor application. ACS Applied Nano Materials, 2025, 8(38), 18701–18714. https://doi.org/10.1021/acsanm.5c04174
37. Kumar, A., Mahanty, B. N., Rawat, A., Muhammad, R., Panigrahi, R. K., Pradhan, D., Mohanty, P. Transition-Metal-Substituted Nanoporous Manganese Ferrites $Mn_{0.95}M_{0.05}Fe_2O_4$ (M: Co, Cu, and Zn) as Electrode Materials for High-Performance Supercapacitors in Redox-Active Nonaqueous Electrolytes. Energy & Fuels 2023, 37, 6810–6823. https://doi.org/10.1021/acs.energyfuels.3c00281.
38. Wei, C., Feng, Z., Baisariyev, M., Yu, L., Zeng, L., Wu, T., Zhao, H., Huang, Y., Bedzyk, M. J., Sritharan, T., Xu, Z. J. Valence Change Ability and Geometrical Occupation of Substitution Cations Determine the Pseudocapacitance of Spinel Ferrite XFe_2O_4 (X = Mn, Co, Ni, Fe). Chemistry of Materials 2016, 28, 4129–4133. https://doi.org/10.1021/acs.chemmater.6b00713.
39. Baruah, P. K., Mukherjee, N., Bhagat, B., Mukherjee, K. Wet Chemical Synthesis of Cubic Spinel Ferrites: A Review Addressing Phase Formation Behavior and Nanostructuring. Crystal Growth & Design 2024, 24, 1504–1528. https://doi.org/10.1021/acs.cgd.3c01039.
40. Vuong, T. T., Nguyen, P. L., Nguyen, N. T., Phung, T. V. B., Le, P.A. Zinc–Carbon Battery Recycling for Investigating Carbon Materials for Supercapacitor Applications. ACS Omega 2024, 9, 22543–22556. https://doi.org/10.1021/acsomega.3c08537.
41. Yang, C., Sun, M., Zhang, L., Liu, P., Wang, P., Lu, H. $ZnFe_2O_4$@Carbon Core–Shell Nanoparticles Encapsulated in Reduced Graphene Oxide for High-Performance Li-Ion Hybrid Supercapacitors. ACS Applied Materials & Interfaces 2019, 11, 14713–14721. https://doi.org/10.1021/acsami.8b20305.